Thermal Barrier Coatings for Diesel Engines

ANDERS THIBBLIN

Licentiate Thesis
KTH Royal Institute of Technology
Machine Design
SE-100 44 Stockholm, Sweden

Stockholm, Sweden 2017

TRITA MMK 2017:11
ISSN 1400-1179
ISRN/KTH/MMK/R-17/11-SE
ISBN: 978-91-7729-475-7

Stockholm, Sweden 2017
Print: Universitetsservice US-AB

Akademisk avhandling som med tillstånd av KTH i Stockholm framlägges till offentlig granskning för avläggande av Teknologie Licentiatexamen fredagen den 8 september 2017 kl. 13:00 i sal B242, KTH, Brinellvägen 83, Stockholm.

Abstract

Reducing the heat losses in heavy-duty diesel engines is of importance for improving engine efficiency and reducing CO_2 emissions. Depositing thermal barrier coatings (TBCs) onto engine components has been demonstrated to have great potential to reduce heat loss from the combustion chamber as well as from exhaust components. The overall aim of this thesis is to evaluate the thermal cycling lifetime and thermal insulation properties of TBCs for the purpose of reducing heat losses and thermal fatigue in heavy-duty diesel engines.

The thermal cycling performance and crack behaviour of different TBCs were evaluated by exposing the coatings to alternating hot and cool gas inside exhaust manifolds, inside the combustion chamber of a diesel engine, and in different types of furnaces. The thermal conductivity of coatings was calculated based on porosity measurements and thermal diffusivity measured using a laser flash apparatus. Directional hemispherical reflectance was measured because thermal radiation may significantly affect heat transport through semi-transparent coatings inside the combustion chamber.

In the thermal cycling test inside exhaust manifolds, different top coat materials fabricated using atmospheric plasma spraying (APS) were evaluated. Nanostructured yttria-stabilized zirconia (YSZ) performed best, followed by YSZ with conventional microstructure and then $La_2Zr_2O_7$. Forsterite and mullite could not withstand the thermal cycling conditions and displayed large cracks or spallation. Two sol-gel composite coatings displayed promising thermal cycling performance results in a furnace test under similar conditions.

Thermal cycling testing of YSZ coatings having different types of microstructure, in a furnace at temperatures up to 800°C, indicated that the type of microstructure exerted a great influence. In the APS coatings, a segmented microstructure resulted in a thermal cycling lifetime 5–10 times longer than that of a nanostructured or conventional microstructure due to the high strain compliance provided by the segmentation cracks. An even longer lifetime was seen for a plasma spray–physical vapour deposition (PS-PVD) coating, in which intercolumnar gaps provide excellent strain compliance.

In situ heat flux measurements inside the combustion chamber indicated that plasma-sprayed $Gd_2Zr_2O_7$ was the TBC material providing the largest heat flux reduction. This is explained by a combination of low thermal conductivity and high reflectance. The plasma-sprayed YSZ and $La_2Zr_2O_7$ coatings provided very small heat flux reductions. Long-term testing indicated a running-in behaviour of YSZ and $Gd_2Zr_2O_7$, with a reduction in heat flux due to the growth of microcracks in YSZ and the growth of macrocracks in $Gd_2Zr_2O_7$.

Keywords

Thermal barrier coatings, diesel engine, thermal cycling fatigue, heat flux, running-in, exhaust manifolds, yttria-stabilized zirconia, gadolinium zirconate, lanthanum zirconate

Sammanfattning

Genom att minska värmeförlusterna är det möjligt att uppnå en högre verkningsgrad för dieselmotorer för tunga fordon. Det har visats att termiska barriärskikt (TBC) på motorkomponenter ger en stor potential för minskning av värmeförluster inne i förbränningsrummet såväl som från avgaskomponenter. Målet med denna avhandling är att utvärdera livslängd i termisk cykling och termisk isoleringsförmåga för termiska barriärskikt, för minskning av värmeförluster och termisk utmattning i dieselmotorer för tunga fordon.

Förmåga att klara av termisk cykling har undersökts genom att utsätta de termiska barriärskikten för omväxlande varma och kalla gaser inne i grenrör, i förbränningsrummet i en dieselmotor, samt i ugnar. Termisk ledningsförmåga har beräknats utifrån porositetsmätningar och värmediffusivitetsmätningar. Spektral total hemisfärisk reflektans har uppmätts, eftersom värmestrålning kan ha en stor inverkan på värmeflödet genom semi-transparenta ytbeläggningar inne i förbränningsrummet.

TBC-skikt bestående av olika material har framställts med atmosfärisk plasmasprutning (APS) och exponerats för termisk cykling inuti avgassamlare. Nanostrukturerad yttriumoxid-stabiliserad zirkoniumdioxid (YSZ) klarade provningen bäst, följt av YSZ med konventionell mikrostruktur och $La_2Zr_2O_7$. Forsterit och mullit klarade inte den termiska cyklingen, utan hade makrosprickor eller avflagningar efter testet. Två kompositbeläggningar framställda med sol-gel-metod visade lovande resultat i ugnsprovning under likande termiska förhållanden som i avgassamlaren.

En stor inverkan av mikrostrukturen på förmågan att klara av termisk cykling kunde påvisas i ugnsprovning för YSZ. För APS-beläggningar klarade en segmenterad struktur 5–10 gånger fler cykler än nanostruktur såväl som konventionell mikrostruktur, på grund av de vertikala sprickornas positiva inverkan på förmågan att klara av töjningar i skiktet. En beläggning som framställts med plasmasprutning – fysikalisk ångdeponering (PS-PVD) klarade ännu fler cykler, vilket kan relateras till dess interkolumnära porositet som ger goda töjningsegenskaper.

In situ mätningar av värmeflödet från förbränningsrummet visade att plasmasprutad $Gd_2Zr_2O_7$ var det termiska barriärskikt med bäst isolerförmåga. Det kan förklaras av en kombination av låg värmeledning och hög reflektans. Plasmasprutad YSZ och $La_2Zr_2O_7$ gav endast små minskningar av värmeflödet. Långtidsprov visade ett inkörningsbeteende för YSZ and $Gd_2Zr_2O_7$. En förbättrad isolerförmåga över tid berodde på tillväxt av mikrosprickor för YSZ, och tillväxt av makrosprickor för $Gd_2Zr_2O_7$.

Acknowledgements

I would like to express my gratitude to my main supervisor Professor Ulf Olofsson for his unstinting support and guidance. I would also like to thank my co-supervisors, Professor Stefan Jonsson and Docent Senad Dizdar, for their great assistance during the project.

I want to acknowledge the generous support of Scania CV AB in financing the projects and enabling me to start my PhD studies. In particular, I would like to thank my group managers over the years, Dr. Jenny Kylefors and Sven-Eric Stenfors. I am grateful to Dr. Jessica Elfsberg, Daniel Norling, Christian Binder, and Dr. Madeleine Ekström for many productive discussions, and to Jan Kron, Lennart Persson, Thomas Hammarlund, and Anders Kjelledal for their help with sample preparation. The work of Christoffer Blomqvist, Salvatore Pisasale, and Siamak Kianzad in their master thesis projects has been of great value for this research. All my colleagues at Scania and KTH deserve thanks for all the interesting discussions and help over the years.

I am grateful to Tech. Lic. Krishna Praveen Jonnalagadda at Linköping University for performing the LCF tests, Jacob Steggo at Jönköping University for performing the thermal diffusivity measurements, Mattias Weibull at Höganäs AB for assisting with the hot hardness measurements, and Tomas Hallberg at FOI, Linköping for performing the optical measurements. Also, I would like to thank Dr. Ralf Rablbauer at VW for many valuable discussions.

Finally, I must thank my wife Sandra for all her support during this period, and my daughters Elin and Agnes for all the joy and laughter they bring.

Stockholm, April 2017

Anders Thibblin

Contents

1 Introduction

List of abbreviations

APS	Atmospheric plasma spraying
CTE	Coefficient of thermal expansion
EB-PVD	Electron beam–physical vapour deposition
DHR	Directional hemispherical reflectance
GZ	Gadolinium zirconate
HCF	High cycle fatigue
LCF	Low cycle fatigue
LFA	Laser flash analysis
LHR	Low heat rejection
LOM	Light optical microscope
LPPS	Low-pressure plasma spray
LZ	Lanthanum zirconate
PS-PVD	Plasma spray–physical vapour deposition
SEM	Scanning electron microscope
SPS	Suspension plasma spray
TBC	Thermal barrier coating
TCF	Thermal cycling fatigue
TEG	Thermo-electrical generators
TGO	Thermally grown oxide
WHR	Waste heat recovery
YSZ	Yttria-stabilized zirconia

Modern heavy-duty diesel engines have an engine efficiency of about 45%, the rest of the energy being used for running auxiliary systems or lost as heat or friction. Heavy-duty vehicles lose on average about 20% of the fuel energy inside the combustion chamber as heat to the coolant and 30% as heat to the exhaust [1]. Because so much of the fuel energy is lost as heat, various technologies that can be used to reduce heat losses have attracted considerable attention, thermal barrier coatings (TBCs) being one of them. TBCs could significantly improve the efficiency of diesel engines, and even a small improvement would have a large impact on the environment, considering the total fuel consumption of heavy-duty vehicles globally. The total annual fuel consumption of heavy-duty trucks and buses was more than 540,000 million litres in 2012, corresponding to CO_2 emissions exceeding 1400 million tonnes [1].

There are various technologies for retrieving heat energy from exhaust: turbocharging is common; waste heat recovery systems (WHRs) based on the Rankine cycle, and turbocompounding can convert heat energy from the exhaust into mechanical work on the crankshaft; and thermo-electrical generators (TEGs) can be placed in the exhaust stream and convert heat energy into electrical energy. Another way of reducing the heat losses is to use TBCs. These coatings, typically ceramic coatings with low thermal conductivity, can be used in exhaust components to keep the heat in the exhaust, or in the combustion chamber to reduce the heat losses to the coolant. Lower heat losses in the combustion chamber can result in higher exhaust temperatures and/or a higher gas pressure and more work on the piston, resulting in higher engine efficiency. This is supported by experimental results of Modi [2], who has studied the energy balance of a thermally insulated small diesel engine (see Fig. 1). Some tests of TBCs on the combustion chamber walls of heavy-duty diesel engines have indicated improvements of 5–6% in brake specific fuel consumption [3, 4]. Thermal barriers also protect the coated components from high temperatures, reducing problems with thermal fatigue and oxidation.

TBCs inside a heavy-duty diesel engine are subjected to rapid thermal cycling from combustion events, and slower but larger temperature cycling from load variations and the start/stop of the engine. Because a heavy-duty truck is expected to last about ten times the mileage of a regular passenger car, this puts high demands on the durability of the coatings.

The alternating hot combustion gases and cool intake air, soot on the walls, and thermal radiation from the flame and hot walls are all factors that influence the heat flux through the TBCs. It is difficult to predict how much thermal insulation a TBC provides based solely on the various material properties evaluated in lab tests. In situ measurements are required in order to determine the actual thermal insulation effect of TBCs inside the combustion chamber of a heavy-duty diesel engine. Performing such measurements and combining them with lab tests of properties such as thermal conductivity and reflectance give an improved understanding of how best to design a TBC to reduce heat losses.

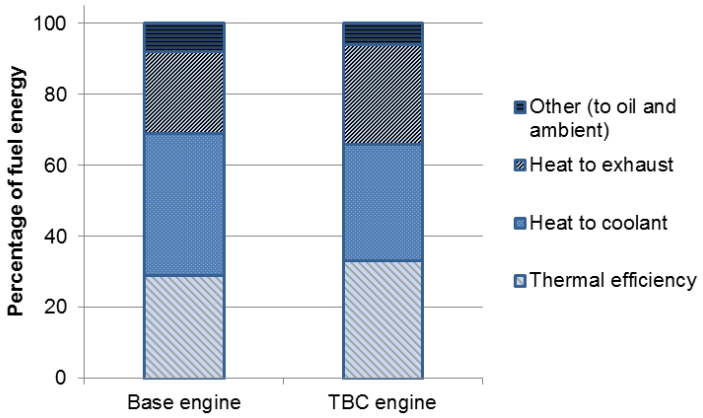

Figure 1: Energy balance at medium load in a small diesel engine with and without thermal barrier coatings on combustion chamber components. Less energy is lost to coolant and more is converted into mechanical power and lost to exhaust with the use of these coatings; adapted from Modi [2].

1.1 Objectives

The overall aim of this thesis is to evaluate 1) the lifetime of TBCs subjected to thermal cycling and 2) the thermal insulation properties of TBCs for the purpose of reducing heat losses and thermal fatigue in heavy-duty diesel engines.

1.2 Research questions

The main research question in this thesis is:

What coating processes and materials for thermal barrier coatings can be used to reduce the heat losses inside the combustion chamber and from exhaust components in a heavy-duty diesel engine?

The main research question has been divided into the following sub-questions:

- What is the thermal cycling performance and crack behaviour of different TBCs for exhaust manifold applications?
- How is the substrate temperature of exhaust components influenced by different TBCs and different coating thicknesses?
- How do different coating microstructures, produced using APS and PS-PVD, influence the thermal cycling lifetime of the TBC?
- How do different coating microstructures, produced using APS and PS-PVD, influence the thermal insulation properties of the TBC?
- How is the heat flux from the combustion chamber influenced by TBCs with respect to their composition, microstructure, and sealed porosity?
- Is there a running-in period, with respect to thermal insulation properties, for TBCs inside a combustion chamber?

1.3 Thesis outline

Chapter 1 gives an introduction to TBCs and the importance of research in this area. Chapter 2 presents how TBCs can be used in diesel engines, what layers a TBC consists of, and what coating processes and coating materials can be used. Chapter 3 presents the challenges that TBCs are subjected to in a heavy-duty diesel engine as well as the possible negative effects of TBCs on engine performance. Chapter 4 describes the investigated TBC materials and the experimental methods used. Chapter 5 presents the results. Chapter 6 discusses the results, followed by the conclusions and proposed future work.

1.4 List of appended publications

Paper A

Madeleine Ekström, Anders Thibblin, Anders Tjernberg, Christoffer Blomqvist, and Stefan Jonsson. "Evaluation of internal thermal barrier coatings for exhaust manifolds", *Surface & Coatings Technology* (2015).
doi: 10.1016/j.surfcoat.2015.04.005
The author was involved in planning the experiments and evaluating the results, and wrote parts of the paper.

Paper B

Anders Thibblin, Siamak Kianzad, Stefan Jonsson, and Ulf Olofsson. "Running-in behaviour of thermal barrier coatings in the combustion chamber of a diesel engine".
Submitted for publication.
The author planned the tests, supervised the design of the heat flux probe, supervised the experimental engine testing work, performed the porosity measurements and most of the microstructural analyses, and wrote the entire paper.

Paper C

Anders Thibblin, Stefan Jonsson, and Ulf Olofsson. "Influence of microstructure on thermal cycling lifetime, thermal insulation, and mechanical properties of yttria-stabilized zirconia thermal barrier coatings".
Submitted for publication.
The author formulated the research questions and chose the methodology for answering them, planned the experimental tests, performed all microstructural analyses, porosity measurements, and Vickers hardness measurements, made the synthesis, evaluated the results of the remaining experiments, and wrote the entire paper.

2 Background

2.1 Low-heat-rejection diesel engines

The first work on TBCs for diesel engines was presented in the mid 1970s by Kvernes [5]. The early researchers examining low-heat-rejection (LHR) engines faced problems with the durability of the ceramic components or coatings, high emissions, and degraded combustion. Many researchers have since studied the effects of TBCs on fuel efficiency and heat losses in diesel engines. In a 2003 literature review, Jaichandar [6] concluded that most experiments with TBCs found a 2–12% reduction in fuel consumption, but some experiments actually found up to 25% increase in fuel consumption. Better results can be expected for turbocharged and turbocompound engines, as these can compensate for the typically decreased volumetric efficiency of an LHR engine and even recover part of the energy in the exhaust [6].

Of the heat losses inside the combustion chamber of a heavy-duty diesel engine, about 50% is transported into the piston, while 40% goes to the cylinder head and 10% to the cylinder liner [7]. The relatively small part of the heat lost to the liner is due to the very small area of the liner that is exposed when the temperature and pressure are at their highest at the beginning of the combustion cycle. The components that have the highest potential for heat loss reduction with the use of TBCs are thus the piston and the cylinder head including the valves.

The fire deck is not the only surface of the cylinder head that it would be useful to insulate. Coating the intake and exhaust ports with TBC would reduce the heating of intake gas and reduce the heat losses from the exhaust to the cylinder head. Decreased heat losses result in more energy left in the gas, heat that can be recovered by turbo-compounding, thermoelectric generators, and Rankine-cycle systems. Other positive effects of having TBCs in the exhaust stream include a shorter time to reach the operating temperature of the exhaust after-treatment systems and improved fuel efficiency by reducing the need for actions to maintain the correct temperature of these systems.

Thermal insulation of the inside of the exhaust and turbo manifolds produces the same types of benefits as does using TBC inside the cylinder head, but also reduces the thermal load on the manifolds. Lower temperatures of the cast iron or steel in the manifolds reduce the risk of thermal fatigue crack formation. In addition, the lower temperatures and the protective coating reduce the oxidation rate of the material in the components. A higher exhaust gas temperature can thus be permitted when using TBC. Some of the components of interest for coating with TBC are shown in Fig. 2.

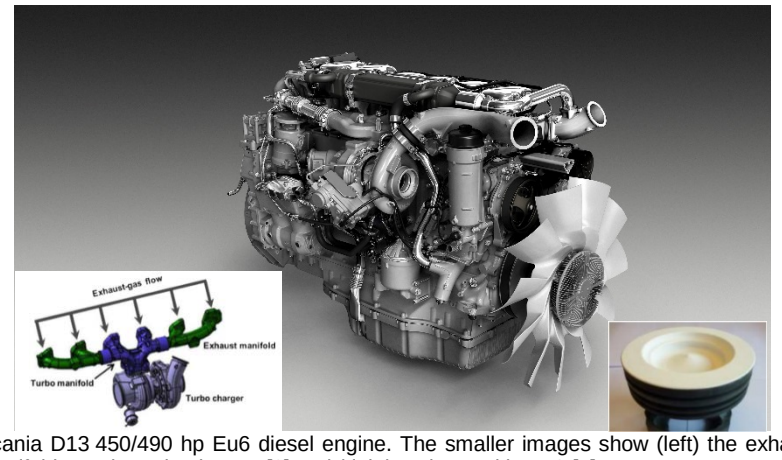

Figure 2: Scania D13 450/490 hp Eu6 diesel engine. The smaller images show (left) the exhaust manifolds, turbo manifolds, and a turbocharger [8] and (right) a piston with TBC [7].

2.2 Thermal barrier coatings

A typical TBC system for diesel engines is shown in Fig. 3. The first layer is the substrate material, which for diesel engine components often is steel, cast iron, or aluminium. The next layer, the bond coat, has two important functions: it should protect the substrate from oxidation and also provide sufficient bonding, often by having an irregular surface that promotes mechanical bonding, for the next layer, the top coat [9, 10]. The top coat, normally consisting of ceramic material, is a low-thermal-conductivity layer that provides the thermal insulation. The thermal conductivity of the top coat can be reduced by various microstructural modifications that reduce the phonon mean free path. During high-temperature exposure, a thermally grown oxide (TGO) layer forms in the interface between the bond coat and the top coat. The coating processes and materials used for the different layers will be further described in the following sections.

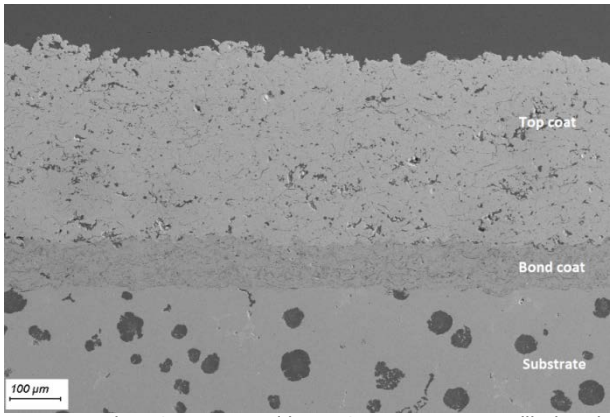

Figure 3: Typical plasma-sprayed TBC system, with a YSZ top coat, metallic bond coat (FeCrAlY), and cast iron substrate (SiMo51).

2.3 Coating processes and microstructures

Several different coating processes can be used to deposit TBCs onto metallic substrates. Some of these coating processes, and typical microstructural features associated with them, are described below.

2.3.1 APS

Atmospheric plasma spraying (APS) is widely used due to its high deposition rate, low cost, ability to coat large components, and high-porosity microstructure that reduces the thermal conductivity [11].

In atmospheric plasma spraying, particles with a diameter of typically 5–50 µm are injected into a plasma jet with a temperature typically in the range of 8000–14,000 K [12, 13]. The total mass flow rate of particles that can be injected into the plasma varies depending on the type of plasma torch used, but is typically 3–20 kg h^{-1} [12]. The particles are heated and accelerated towards the substrate by the plasma jet. On impact, the molten particles flatten and form splats (see Fig. 4). As more splats hit the surface, a lamellar coating is built up. The cooling rates during solidification of the splats can exceed 10^5 K s^{-1}, leading to directional solidification and grain growth mainly perpendicular to the substrate [13, 14].

The microstructure of APS coatings can be modified by changing, for example, the feedstock composition and morphology, plasma gas composition and gas flow, and substrate temperature [11, 13]. Three types of APS microstructures – conventional, nanostructured, and segmented – will be discussed below.

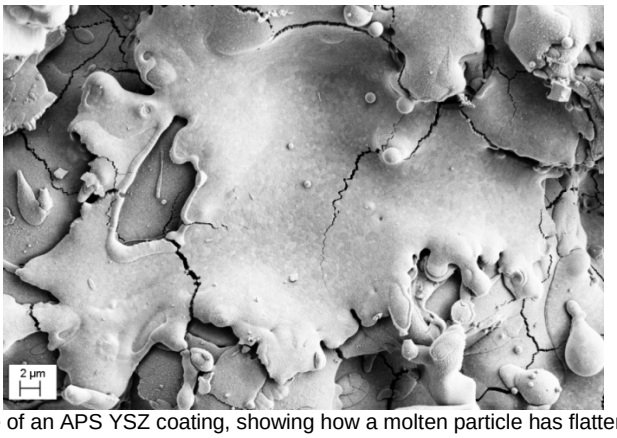

Figure 4: The surface of an APS YSZ coating, showing how a molten particle has flattened on impact.

2.3.1.1 APS, conventional

Plasma-sprayed TBCs with conventional microstructure typically have 10–15% porosity [15]. The porosity consists of various types of pores and cracks (see Fig. 5). Large pores form when splats do not completely fill the holes between previously sprayed particles [11, 16]. Intersplat pores and cracks are caused by factors such as shadowing by previously deposited particles and splat-curling caused by surface tension and thermal expansion mismatch stresses [16]. Intrasplat cracks are caused by stresses from the rapid cooling of the splats, from the cooling of the entire coating, and from solid-state phase transformations [17]. The porosity provides some lateral strain compliance for APS coatings with conventional microstructure [9].

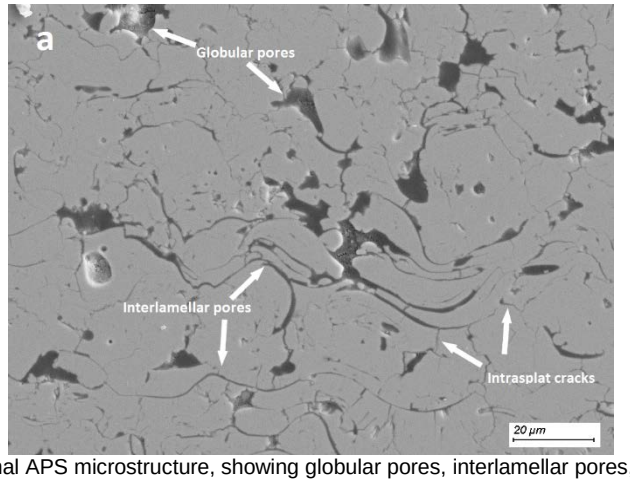

Figure 5: Conventional APS microstructure, showing globular pores, interlamellar pores, and intrasplat cracks.

2.3.1.2 APS, nanostructured

Using nanostructured, agglomerated feedstock particles, a microstructure comprising semi-molten particles surrounded by fully molten particles (see Fig. 6) can be built up with plasma spraying [18]. This type of microstructure, with nanozones embedded in a conventional microstructure, is often referred to as a “nanostructured” or “bimodal” microstructure [18].

Improved thermal cycling lifetime [19–21] and decreased thermal conductivity [18, 19, 22] compared with those of conventional microstructure have been reported. Lower residual stresses and a lower elastic modulus in nanostructured coatings can explain their better thermal cycling lifetime [20]. The low thermal conductivity of nanostructured coatings can be attributed to higher porosity [19] and increased phonon scattering due to the increased extent of grain boundaries [23, 24] and submicron porosity [23]. The reduced thermal conductivity due to decreased grain size is most noticeable at low temperatures, while this effect is insignificant at high temperatures [25]. The mean free path of the phonons decreases with temperature, until it is limited by the interatomic spacing. The grain boundaries therefore do not limit the phonon mean free path unless the grain boundaries are opaque to phonon transmission. For tetragonal zirconia, which is not opaque to

phonon transmission across the grain boundaries, the thermal conductivity is not grain-size dependent at temperatures above 1000°C [25]. However, at the significantly lower temperatures in a diesel engine, grain size may be an important factor reducing the thermal conductivity of the top coat.

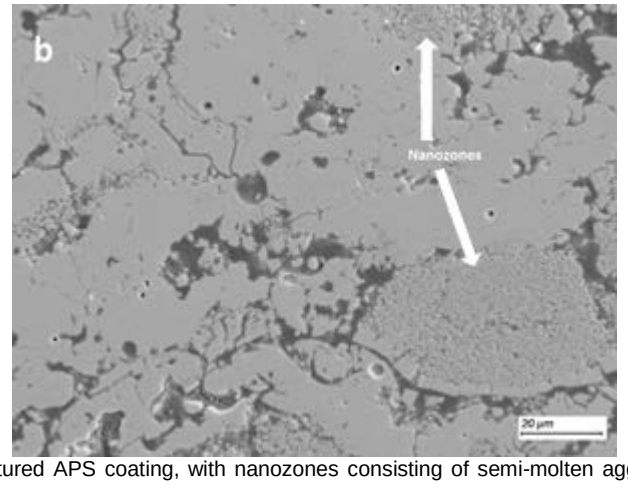

Figure 6: Nanostructured APS coating, with nanozones consisting of semi-molten agglomerated particles that are surrounded by splats formed by fully-molten particles.

2.3.1.3 APS, segmented microstructure

Segmentation cracks are vertical cracks that run perpendicular from the surface (see Fig. 7) to a depth of at least 50% of the top coat thickness [13]. TBCs with such segmentation cracks can be manufactured using the APS process by adjusting the spray parameters. As described in section 2.3.1, the solidification rate is very high when plasma spraying ceramics, which leads to solidification directed from the substrate towards the surface. If the coating surface is kept at a relatively high temperature, increased diffusion will improve the bonding between the splats, increase the grain size, and promote the growth of microcracks over several splats [13, 26]. A high feeding rate or low relative speed between the spray gun and the coated specimen can be used to obtain higher pass thickness, which also promotes the growth of larger grains and vertical cracks [13]. A large temperature gradient between the surface and the particles hitting the surface is also required when spraying segmented coatings [13].

Exposure of TBCs to high temperatures leads to tensile stresses in the top coat, caused by thermal expansion mismatch between the different coating layers, and to stress relaxation [13]. The vertical cracks in the segmented coating can open up during the high-temperature stage, which reduces the tensile stresses in the top coat [13, 26]. This gives a lower stress relaxation during high-temperature exposure, leading to lower compressive stresses in the coating during the ensuing cooling stage, which are positive for the coating lifetime [13]. Thermal cycling tests have demonstrated that the improved strain tolerance due to the segmentation cracks gives a longer coating lifetime than that given by conventional APS microstructure [13, 26, 27].

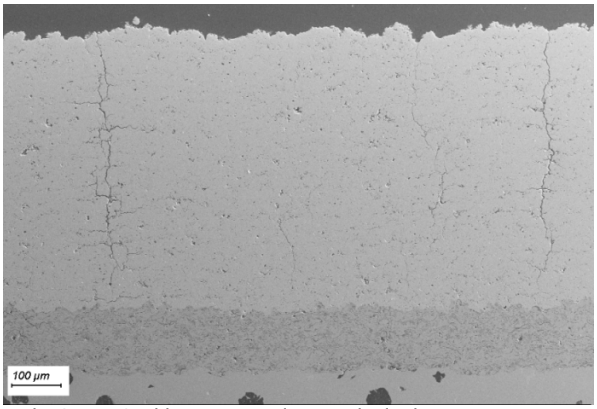

Figure 7: Plasma-sprayed YSZ TBC with segmentation cracks in the top coat.

2.3.2 EB-PVD

Electron beam–physical vapour deposition (EB-PVD) coatings have a columnar microstructure with inter-columnar gaps (see Fig. 8) that permit lateral strain compliance [9]. EB-PVD coatings are often used on mechanically loaded parts in aero and industrial turbines. The part to be coated is preheated and inserted into a vacuum chamber, where electron beams melt and evaporate ceramic ingots. The vapour, mixed with a controlled amount of oxygen, is deposited onto the substrate at rates of 4–10 µm min^{-1} [28]. This is an expensive coating process and, due to high deposition temperatures of about 1000°C [29], cannot be used with many of the alloys used for diesel engine components, as these may either melt or undergo phase transformations.

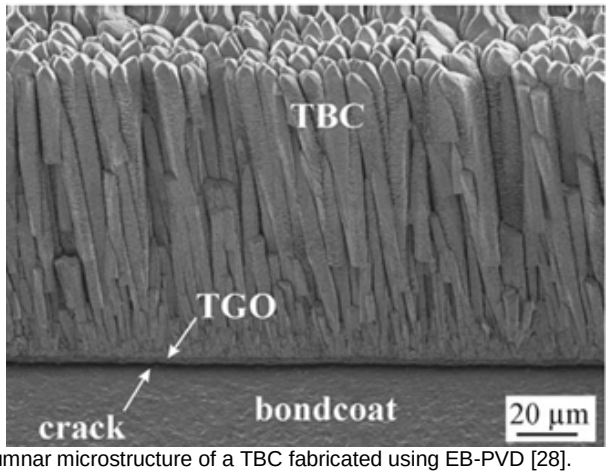

Figure 8: Typical columnar microstructure of a TBC fabricated using EB-PVD [28].

2.3.3 PS-PVD

Plasma spray–physical vapour deposition (PS-PVD) is a relatively new process that combines some of the main advantages of both the APS and EB-PVD processes. A columnar microstructure, similar to that of EB-PVD coatings, can be produced by the PS-PVD process [30] (see Fig. 9). This type of microstructure, with featherlike columns separated by gaps, provides a high strain tolerance [30, 31]. Because it is a plasma spray process, it is lower in cost and has a higher deposition rate than the EB-PVD process [32].

The spraying distance in the PS-PVD process can be more than 2 m and the plasma plume can be 0.4 m wide [12]. The long spraying distance, low pressure (about 0.1 mbar) in the PS-PVD chamber, and high power of the plasma gun allow evaporation of the injected powder [31, 32]. When the vapour reaches the surface, a columnar structure layer starts to grow. Crystals of certain orientations grow faster and create columns, while the slower-growing crystals stop growing when they reach another column [33]. Gaps between the columns are then created, leading to the high strain tolerance of the coating.

For PS-PVD coatings, the thermal conductivity is reportedly about 1.1 $Wm^{-1} K^{-1}$ at 1200°C for those with quasi-columnar microstructure [31], and 0.8 $Wm^{-1} K^{-1}$ at temperatures up to 1000°C for those with columnar microstructure [32]. These low values are explained by the high porosity and large number of defects in the microstructure [31, 32].

The substrate normally has a temperature of about 900–1100°C during the PS-PVD process [32], which is too hot for many materials used for diesel engine components.

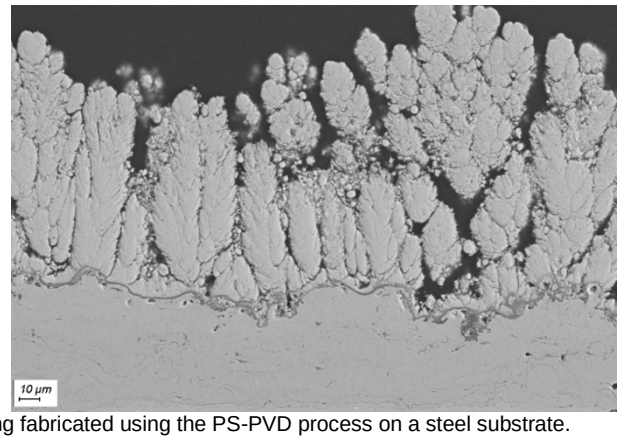

Figure 9: YSZ coating fabricated using the PS-PVD process on a steel substrate.

2.3.4 Sol-gel and slurry coatings

Slurry spraying is a relatively cheap and simple method for producing TBCs [34]. The slurry, which consists of powder suspended in a fluid, is applied to a surface in several layers using a spray gun. After drying, the multilayer coating is pressed in a compression chamber, followed by sintering in a furnace or with an acetylene torch [34]. A great advantage of this coating method is the ability to coat complex geometries, including surfaces inside pipes that are out of direct sight [34]. Slurry coatings can also be applied by dipping the substrate in a mixture of ceramic powder and then leaving it to dry. This is repeated until the desired thickness has been reached, after which the coating is densified by hot isostatic pressing [35].

The sol-gel process is another non-line-of-sight process. First, a solution typically consisting of metal alkoxides in an organic solvent is formed. A sol-gel coating can be manufactured by spraying the solution or dipping the substrate in it, followed by gravitational draining and evaporation of the solvent [36]. A firing process then compacts the dried sol into a hard oxide coating. A sol-gel coating with incorporated ceramic particles is shown in Fig. 10.

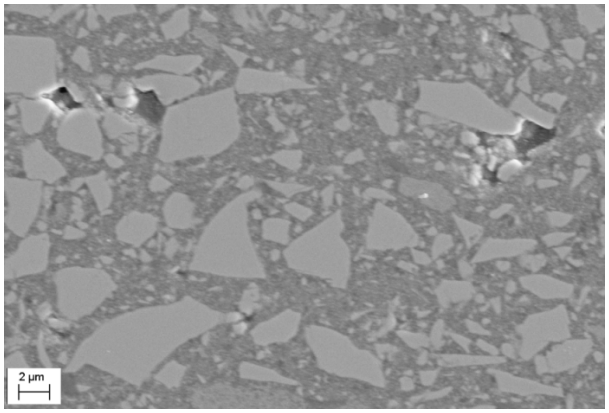

Figure 10: Sol-gel composite TBC, showing CaSZ (large particles) and YSZ (small particles) in a silica matrix.

2.4 Top coat materials

A top coat material to be used in a diesel engine must fulfil a number of requirements [9, 37]:

- low thermal conductivity
- low specific heat
- thermal expansion close to that of steel and cast iron
- strain compliance, because thermal expansion mismatch between the layers of a TBC system causes large strains during thermal cycling
- thermodynamic compatibility with the oxides that form in the interface between the top coat and the bond coat
- high flexural strength

- high fracture toughness
- high thermal shock resistance

The top coat can consist of a single layer or of several layers to combine the desired properties of different materials. For example, a first layer that provides toughness during thermal cycling could be combined with a second layer that protects the TBC from the infiltration of calcium-magnesium-alumino-silicates (CMASs) [38]. TBCs can also have graded structures, as they can effectively reduce thermal stresses in the coating [35].

Several different top coat materials have been evaluated over the years for diesel engine applications. Some of these materials will be discussed in this section.

2.4.1 YSZ

The ceramic most often used as a top coat in aero and industrial turbines, and in diesel engine tests, is yttria partially stabilized zirconia (YSZ). Pure zirconia, ZrO_2, possesses many of the required properties listed above, but undergoes detrimental tetragonal-to-monoclinic phase transformation during cooling. This is associated with an increase in volume of approximately 3–5% [39], which may result in coating failure. Zirconia is therefore normally stabilized with 6–8 wt% yttria (Y_2O_3). With these yttria contents, YSZ coatings have compositions placing them in a two-phase region of the phase diagram, where yttrium-lean tetragonal and yttrium-rich cubic phases are found (see Fig. 11). However, due to rapid cooling during the coating processes, a metastable t´ phase is formed instead of the two-phase mixture. When subjected to high temperatures, the t´ phase is decomposed through diffusion into a two-phase mixture of the tetragonal and cubic phases [10]. This may cause spallation of the coating due to volume change when the tetragonal phase later transforms to the monoclinic phase. However, the t´ phase can be expected to be stable at the relatively low temperatures in a diesel engine.

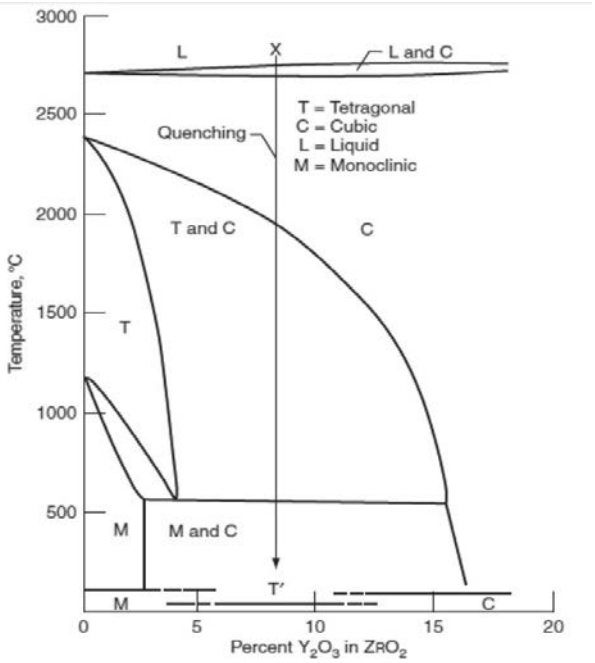

Figure 11: Phase diagram of yttria-stabilized zirconia [41, 42].

Additions of yttria or other stabilizers result in a significant number of vacancies, which are effective in scattering phonons and reduce the thermal conductivity of the material [28]. The type of deposition process also greatly influences the thermal conductivity of the coating. For 6–8 wt% YSZ, the thermal conductivity is typically 1.8–2.0 $Wm^{-1}\ K^{-1}$ for EB-PVD coatings and can be as low as 0.9 $Wm^{-1}\ K^{-1}$ for plasma-sprayed coatings [28]. The coefficient of thermal expansion (CTE) is $10.7 \times 10^{-6}\ K^{-1}$ for plasma-sprayed YSZ with 7.8 wt% Y_2O_3 in the 30–1000°C temperature interval

[40]. This is close to the CTE of steel and cast iron. A close CTE match is important in reducing the stresses during thermal cycling.

2.4.2 $Gd_2Zr_2O_7$

Gadolinium zirconate ($Gd_2Zr_2O_7$, GZ) is a ceramic with a pyrochlore structure. Gadolinium zirconate has excellent thermal stability and can be used at temperatures above 1300°C [43]. The thermal conductivity of a plasma-sprayed GZ coating is about 20% lower than that of plasma-sprayed YSZ [44]. It has been demonstrated that GZ reacts with alumina in the TGO to form $GdAlO_3$, which may compromise the oxidation protection provided by the TGO [45]. To prevent this reaction, it is recommended that a diffusion barrier, such as YSZ, be used or that the temperature near the TGO be kept well below 1100°C [45]. Because bond coat temperatures in diesel engines in general are much lower than 1100°C, this might not be a problem for such applications.

2.4.3 $La_2Zr_2O_7$

Lanthanum zirconate (LZ, $La_2Zr_2O_7$) is another ceramic with a pyrochlore structure. Its fracture toughness is comparable to that of YSZ and its thermal conductivity is about 20% lower than that of YSZ at elevated temperatures [40]. Other properties that make lanthanum zirconate interesting as a top coat is its low sintering tendency and high-temperature stability up to 2000°C [40, 43].

The thermal expansion of lanthanum zirconate is $9.1 \times 10^{-6}\ K^{-1}$ at 30–1000°C, which is lower than that of YSZ and may lead to higher stresses in the coating due to a larger thermal expansion mismatch with other layers in the TBC system [40, 43]. However, the results of thermal cycling tests of LZ and YSZ/LZ coatings have been promising [40, 43].

When materials are being plasma sprayed, constituents can be lost. In the case of $La_2Zr_2O_7$, La_2O_3 easily evaporates, which may lead to monoclinic and cubic ZrO_2 in the coating [46]. As was described in the section about YSZ, pure ZrO_2 may undergo phase transformations at elevated temperatures, which may cause spallation of the coating. At high temperatures (1400°C), LZ has been observed to react with Al_2O_3, which exists in the TGO layer [46]. However, no reaction was seen at lower temperatures, so this is not expected to be a problem in diesel engine applications.

Ionic conductivity is much lower for LZ than for YSZ [46]. Oxygen is not as easily transported though the top coat, so the bond coat oxidation rate can be expected to be lower.

2.4.4 Mullite

Some top coat materials that have insufficient temperature stability for turbine applications may still be of interest for diesel engines, due to their lower temperatures. One such material is mullite ($3Al_2O_3{\cdot}2SiO_2$). It has been demonstrated that plasma-sprayed mullite contains amorphous phases, which crystallize and decrease in volume at temperatures of 750–1000°C [47, 48]. This volume contraction, along with a low thermal expansion ($4.5 \times 10^{6}\ K^{-1}$ between RT and 1400°C [49]), may lead to cracks in the top coat and to spallation [47, 50]. The crystallization also increases the thermal conductivity of mullite. The room temperature thermal conductivity of a plasma sprayed coating increases from about 1.3 to 1.8 $Wm^{-1}K^{-1}$ after one heating cycle to 1000°C [51].

However, issues with spallation and increased thermal conductivity due to crystallization during high-temperature exposure can be avoided in diesel engines, where coating temperatures are fairly low. Lab tests as well as thermal cycling tests of pistons have indicated that mullite top coats have less surface cracking and last longer than do zirconia top coats [52–54]. The small number of surface cracks is due to the low relaxation of mullite at high temperatures and because compressive stresses can be maintained throughout the cooling cycle [54, 55].

2.4.5 Forsterite

Forsterite ($MgO \cdot 2SiO_2$) has a thermal expansion coefficient $11.0 \times 10^{-6}\ K^{-1}$ between 25 and 800°C [56]. The small thermal expansion mismatch between forsterite and 80Ni-20Cr bond coat with steel

substrate has led to good results in thermal cycling tests [56]. Thermal conductivity decreases with temperature, declining from about 1.8 $Wm^{-1}K^{-1}$ at RT to 1.3 $Wm^{-1}K^{-1}$ at 1000°C [51].

2.5 Substrate material

The substrate material on which the TBC is applied can be of several different types in heavy-duty diesel engines. Some pistons are made of aluminium, although steel is more common. The cylinder head is typically made of cast iron, with either lamellar or compacted graphite. Exhaust manifolds are often made of nodular cast iron, with additions of silicon and molybdenum to improve the thermo-mechanical fatigue and oxidation properties. Cast steel can also be used for these components.

2.6 Bond coat material

For steel and cast iron substrates, bond coats are usually thermally sprayed alloys of type MCrAlY, where M stands for Fe, Ni, Co, or a combination of these elements.

One purpose of the bond coat is to provide sufficient bonding to the top coat [9, 10]. However, because oxygen can easily pass through many top coats (e.g., the commonly used YSZ top coat) at high temperatures, an oxygen barrier is needed to protect the substrate. The bond coats are therefore designed to form a protective α-Al_2O_3 layer in the interface between the bond coat and the top coat [57]. Alumina grows very slowly at high temperatures due to its low oxygen diffusivity. The alumina layer is often referred to as thermally grown oxide (TGO).

Yet another important role of the bond coat is to reduce stresses in the top coat. A ductile bond coat can reduce crack growth near the bond coat/top coat interface [58].

The lower temperatures in diesel engines than, for example, gas turbines, allow the use of a TBC without any bond coat [9] or a bond coat with lower oxidation resistance. FeCrAlY alloys have been suggested as possible bond coats in diesel engines [59, 60].

2.7 Thermal properties

2.7.1 Intrinsic thermal conductivity

The thermal conductivity, K, of insulating solids can be expressed as:

$$K = \frac{1}{3} C v l \tag{1}$$

where C is the heat capacity per unit volume, v is the phonon velocity, and l is the mean free path of the phonons [39, 61]. According to the Dulong-Petit law, C reaches a constant value of $3k_B$ at temperatures above the Debye temperature, where k_B is the Boltzmann's constant. This gives:

$$K = k_B v l \tag{2}$$

The minimum thermal conductivity, K_{min}, of the solid can then be calculated [39, 61]. The velocity of the sound in the material can be used as an approximate value of the mean phonon velocity, v_{min}:

$$v_{min} \sim 0.87 \sqrt{\frac{E}{\rho}} \tag{3}$$

where E is the elastic modulus and ρ is the density. The dimension of the molecule determines the minimum phonon mean free path, l_{min}, according to:

$$l_{min} = \left(\frac{N_A m \rho}{M} \right)^{\frac{2}{3}} \tag{4}$$

where N_A is Avogadro's number, M is the molar mass, and m is the number of atoms per molecule. Combining equations 2–4 then gives:

$$K_{min} = 0.87 k_B \left(\frac{N_A m \rho}{M}\right)^{\frac{2}{3}} \left(\frac{E}{\rho}\right)^{\frac{1}{2}} \quad (5)$$

This indicates that the minimum thermal conductivity can be altered in various ways [39]. Adding alloying elements will influence the molar mass and density, and therefore change the minimum thermal conductivity of the solid. Using novel oxide ceramics will influence the molar mass, number of atoms per molecule, density, and also the elastic modulus. The calculated and experimental minimum thermal conductivities of various TBC materials are shown in Fig. 12.

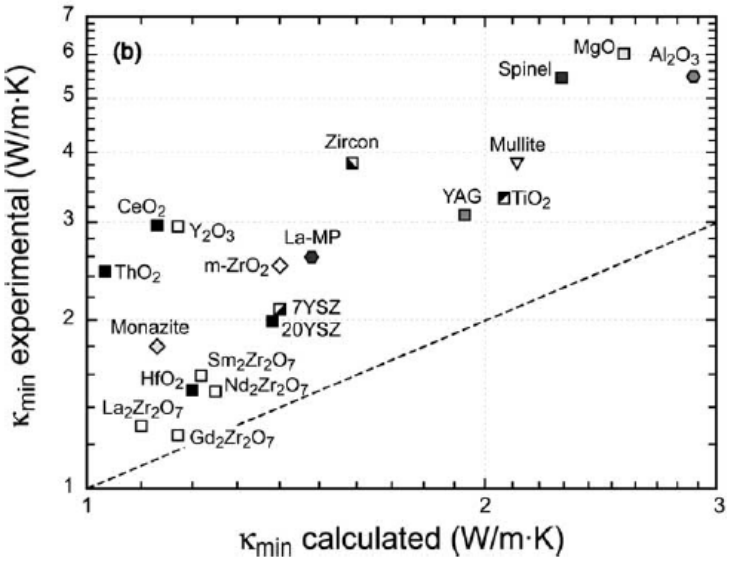

Figure 12: Minimum thermal conductivity values of TBC materials and other ceramics [62].

2.7.2 Influence of microstructure

The thermal conductivity of a solid can be reduced by various modifications of the microstructure. Introducing high porosity and microcracks oriented perpendicular to the heat flux, as is the case for the interlamellar cracks in an APS coating, are effective ways to reduce the thermal conductivity. EB-PVD coatings with microstructural modification that have been successful in reducing the thermal conductivity include a zig-zag structure in the top coat [63] and a multi-layer coating in which YSZ layers are separated by thin Al_2O_3 or Ta_2O_5 layers [64].

3 Challenges for TBCs in a heavy-duty diesel engine

This chapter presents the requirements for TBCs in a diesel engine and the potential problems they could cause during engine operation.

TBCs are exposed to a harsh environment in a diesel engine, where they must withstand the temperature variations from the combustion (see Fig. 13) and start/stop of the engine, high pressures, and a corrosive environment. The high temperature of the flame means that the TBCs must not only have low thermal conductivity, but also optical properties that reduce the radiative heat transport through the coating.

The introduction of TBCs in a diesel engine may influence the combustion characteristics, volumetric efficiency, and emissions. These factors are not investigated in this research, but are introduced in this chapter to give an overview of the problems that may be encountered in an insulated engine.

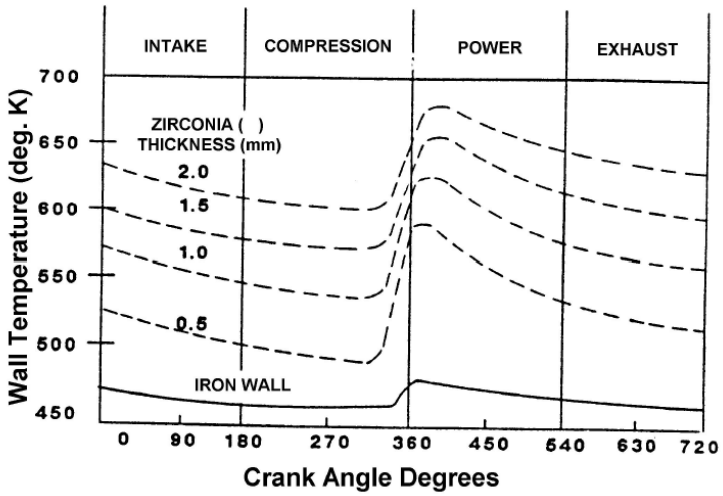

Figure 13: Surface temperatures of combustion chambers with zirconia coatings of different thicknesses [3].

3.1 Durability

TBC durability is an important issue. Heavy-duty trucks often need to run 1–2 million km before being taken out of use. If TBCs fail before that, the engine may be severely damaged. Thermal protection of the substrate is lost, which can cause problems with oxidation, thermal fatigue, and fractured components. A spalled TBC can cause problems for the turbocharger, as large flakes of TBC can damage the turbine wheel blades. Particles from a spalled TBC may also cause excessive wear of the cylinder walls and, if bypassing the piston rings to the oil sump, wear of bearings and other components.

Spallation is generally caused by high stresses in the bond coat/top coat interface, causing crack initiation and growth [28]. These stresses are caused by TGO growth, differences in thermal expansion between different layers, mechanical load, etc. These and other factors, such as sintering and phase transformations, that may cause spallation problems will be discussed below.

3.1.1 Stresses from the coating process

The coating process and thermal cycling conditions during operation generate stresses in the coating; these stresses may cause crack initiation and growth, and eventually coating failure.

Quenching stresses arise in APS coatings during the thermal spraying process. The impacted particles solidify rapidly, but their contraction is restricted by adherence to the underlying coating layers. As a result, tensile quenching stresses form in the coating [57]. CTE mismatch between the

coating and substrate causes stresses in the coating during cooling after spraying. These thermal mismatch stresses in the coating are typically compressive, because the ceramic usually has a lower CTE than does the metallic substrate and therefore shrinks less [57].

3.1.2 Thermal stresses

Thermal expansion mismatch between the different layers in the TBC system causes stresses in the coating during thermal cycling. The ceramic top coat has a lower thermal expansion than does the metallic substrate, which results in tensile stresses in the top coat during heating. When the TBC is held at high temperatures, creep and stress relaxation reduce the magnitude of the tensile stresses, giving rise to compressive stresses in the coating during cooling. The magnitude of the compressive stresses tends to increase with each successive cycle, and may eventually result in coating failure [65]. The TGO growth also results in compressive stresses. The combined effect of these factors is illustrated in Fig. 14.

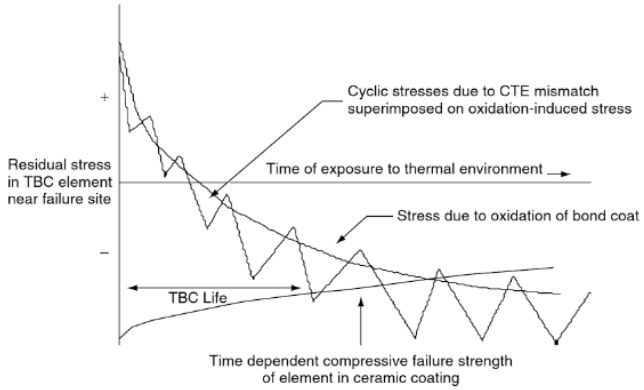

Figure 14: Stress evolution during thermal cycling. The coating fails when the stress equals the bond strength [39].

3.1.3 Sintering, densification, and ageing

Exposure of plasma-sprayed coatings to high temperatures closes the microcracks between the splats in the coating, resulting in the pores being spheroidized [9]. The driving force of this sintering and densification of the TBC is the reduction in surface energy associated with the spheroidization of pores [9].

Some important aspects to be considered when densification occurs are the increase in thermal conductivity over time [9] and risk of spallation due to the volume decrease in the top coat [10]. Another aspect to consider is the decrease in strain compliance. Porous coatings can have good strain compliance due the low elastic modulus associated with high porosity [9, 66]; consequently, densification will lead to decreased strain compliance.

Because densification is temperature dependent, the service temperature and the thermal conductivity of the coating are important factors to consider. Low thermal conductivity will result in large temperature gradients within the coating and, if the service temperature is high enough, large density gradients as well due to densification [9]. The part of the TBC where densification is most likely to occur is the outermost top coat closest to the high-temperature gas.

The increase in thermal conductivity due to sintering can be significant at elevated temperatures [67]. The sintering of microcracks at the splat interfaces together with decreased porosity have been identified as the main reasons for the large increase in the thermal conductivity of coatings after high-temperature exposure [39, 67, 68].

3.1.4 Phase stability/transformations

High-temperature exposure can cause the crystallization of amorphous phases or the phase transformation of top coats, as described in section 2.4. This often leads to a volume change, as in the cubic-to-monoclinic phase transformation of YSZ, which causes a volume increase of 3–5% [39].

A volume change often leads to a risk of failure due to the formation of cracks in the TBC. At the moderate temperatures in diesel engines, YSZ should not undergo phase transformations; however, if other materials are used as the top coat, this factor needs to be considered.

3.1.5 Bond coat oxidation

Oxygen is easily transported through YSZ at elevated temperatures and reacts with the bond coat. Preferably, a slow-growing α-alumina layer, TGO, is formed in the bond coat/top coat interface. The oxidation of the bond coat is associated with growth stress.

Evans [69] has analysed the stresses caused by a fast-growing TGO and noted that large out-of-plane tensile stresses form on the flanks of protuberances in the bond coat/top coat interface; Evans also noted that these stresses are likely to cause the nucleation of cracks, while strain energy in the top coat contributes to the final failure. In aircraft turbine engines, the critical TGO thickness is typically 6–7 µm [39].

3.2 Thermal radiation

YSZ, which is the most common TBC top coat material, is partially transparent to thermal radiation (see Figs. 15–16) [70, 71]. Thermal conductivity typically decreases with temperature, but thermal radiation is proportional to T^3 [72]. At high temperatures, transparency to thermal radiation may thus be an important factor to consider. The bond coat or substrate can be directly heated by external radiation if a translucent TBC is used [70]. Also, thermal radiation generated within the top coat will transport heat from the hotter outer parts of the coat near the surface towards the substrate [70]. The energy balance of a TBC in a diesel engine is shown in Fig. 17.

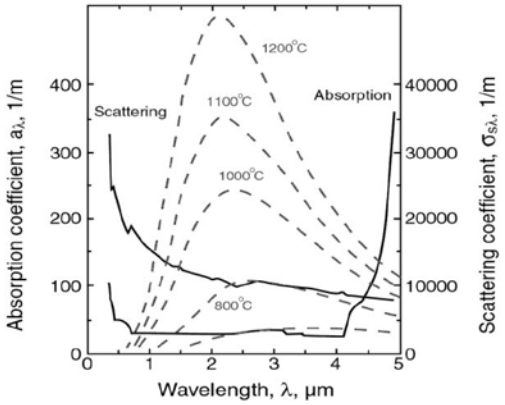

Figure 15: The optical scattering and absorption coefficients of YSZ as well as black-body radiation at several temperatures. The absorption coefficient is low at most wavelengths generated in an engine. Much of the radiation that is not reflected is therefore transmitted through the coating [9].

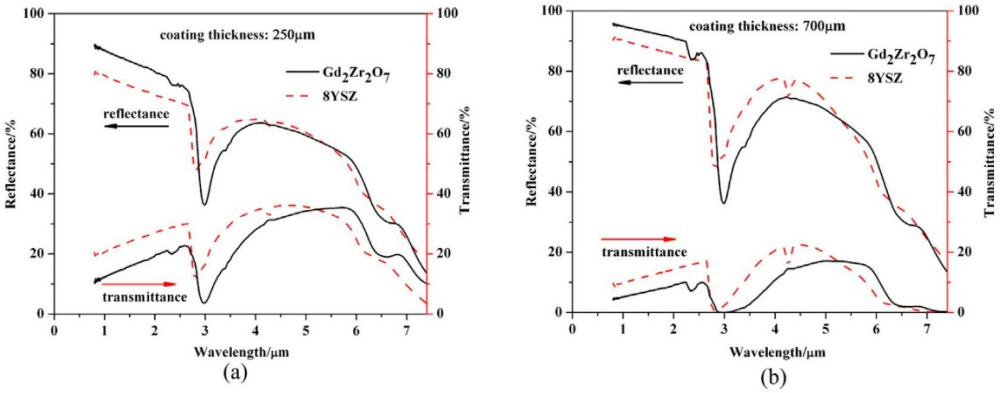

Figure 16: Reflectance and transmittance of GZ and 8YSZ coatings with thicknesses of (a) 250 µm and (b) 700 µm [77].

A highly reflective top coat would reduce the problems with external radiation heating the substrate. It has been demonstrated that adding a thin, reflective aluminium film on top of YSZ reduces the temperature beneath the TBC [73]. In turbine applications, it has been argued that a highly reflective surface layer would be the most effective way to reduce the radiative heat transfer, but that it would be difficult for such a layer to withstand the erosion in that application [9]. Metallic coatings on the surface or embedded in the ceramic may also lead to problems, due to thermal expansion mismatch or poor bonding between the metal and the ceramic [74]. Others have successfully improved the reflectance by coating with multiple layers of YSZ and Al_2O_3 using EB-PVD [75].

Instead of increasing the reflectance, attempts have been made to increase the absorbance of TBCs by incorporating NiO into the coating [9]. However, those attempts were not very successful as they caused an increase in both the thermal conductivity and sintering rate.

Modifying the microstructure can also improve the reflectance. Imperfections, such as microcracks and pores, increase the scattering within the coating, resulting in less radiation transmitted to the substrate and consequently a higher reflectance [74, 76].

In a diesel engine, high reflectance is expected to be important inside the combustion chamber, where thermal radiation is generated from the flame and hot walls. Inside exhaust components, where the TBC thermal radiation is coming only from the hot gases and walls, the reflectance is expected to be less important.

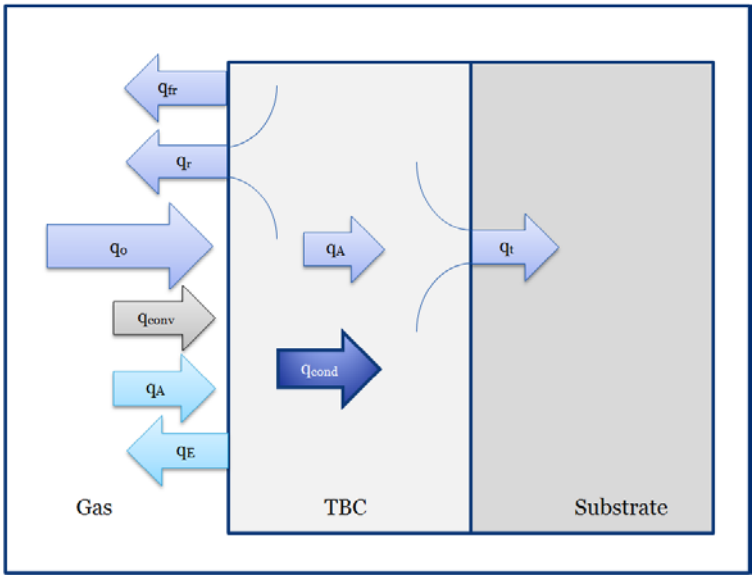

Figure 17: Physical model of the energy balance of a TBC in a diesel engine. The TBC is exposed to heat flux from thermal radiation of short wavelength from the combustion, q_0, and of long wavelength from the hot gas, q_A; it also experiences convective heat transfer from the gas, q_{conv}. Thermal radiation is reflected by the surface, q_{fr}, reflected within the coating, q_r, absorbed within the coating, q_A, and transmitted, q_t, to the substrate. There is also a conductive heat flux within the coating, q_{cond}, and a radiative heat flux from the hot TBC surface, q_E; adapted from Merzlikin et al. [78].

3.3 Emissions

The higher surface temperatures in an insulated engine influence the amount of emissions. The formation of nitrogen oxides, NO_x, is highly temperature dependent. Engines with TBCs could therefore be expected to produce more NO_x, but experimental studies have produced varying results. Some researchers measured increased NO_x and attributed this to higher temperatures, while others measured lower NO_x, which they attributed to, for example, decreased premixed combustion [6].

Hydrocarbon emissions are expected to decrease in an insulated engine due to a smaller quenching distance near the walls and also because of an increased lean flammability limit [6, 37]. The oxidation reactions are helped by the higher temperatures in the combustion chamber, with less unburned hydrocarbon as a result. This is confirmed by most experimental studies [6].

3.4 Influence on combustion characteristics and volumetric efficiency

The theoretical increase in fuel efficiency from applying TBCs to combustion chamber components is often difficult to achieve in practice. Some potential problems associated with TBCs in the combustion chamber are a lower heat release rate, fuel entrapment in pores, increased convective heat transfer, and decreased volumetric efficiency. These issues will be discussed below.

3.4.1 Heat release rate

A lower heat release rate has been reported from several engine tests with thermal insulation [6, 73, 79, 80], which results in decreased fuel efficiency. The low heat release rate may be caused by shorter ignition delays due to the higher temperatures in the insulated combustion chamber. This would result in less fuel being burnt during the premixed combustion and more being burnt during the diffusion phase, shifting the heat release towards the later part of the cycle and giving less useful work on the piston. An example of the shift in heat release is shown in Fig. 18.

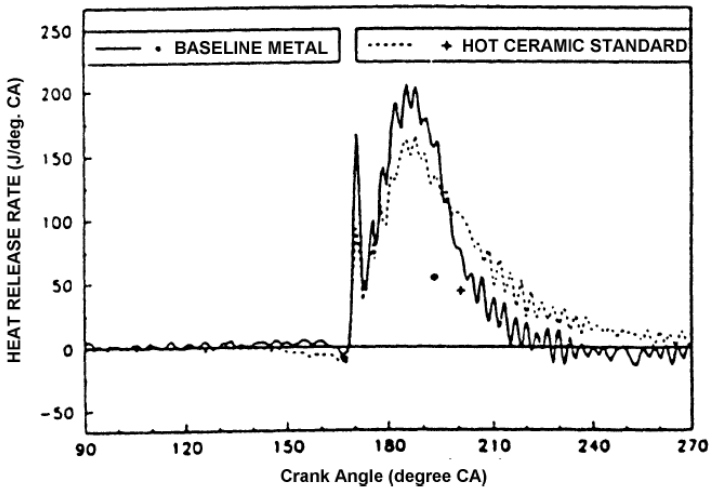

Figure 18: A lower maximum heat release rate and a shift towards the later part of the cycle in a thermally insulated engine [81].

3.4.2 Fuel and air entrapment in pores

The ceramic top coat is porous, which allows air and fuel to penetrate into the coating, especially during the combustion stroke when the pressure can exceed 200 bars in the combustion chamber. Entrapment of fuel in the coating would lead to worsened fuel efficiency, as less fuel may be combusted in the early stage of the combustion stroke. Hot air pushed into the pores would transfer heat from the air into the coating, to a certain distance below the surface. To minimize the effect of fuel and air entrapment, a sealing coating can be used. There are several methods to produce a sealing layer: a dense layer can be applied by thermal spraying onto the ceramic top coat [38], porosity can be sealed by penetrating dip processes, or an organometallic coating can be applied by chemical vapour deposition processes [66]. Yet another method is to apply a film of phosphate glass onto the TBC surface and cure it at 250°C [66].

3.4.3 Volumetric efficiency

Volumetric efficiency is defined as the amount of fresh air trapped in the combustion chamber divided by the theoretical maximum amount of air in the cylinder [82]. TBCs may have a negative effect on the volumetric efficiency, because the intake air is heated by the hotter walls in a thermally insulated combustion chamber and because of the higher residual gas temperature than in a

standard engine [6]. The density of the intake air is decreased and less air can enter the combustion chamber, meaning that the volumetric efficiency drops [2, 6]. Increased turbocharging can be used to maintain high volumetric efficiency [2, 6].

3.4.4 Increased convective heat transfer coefficient

In some tests, insulated walls have actually appeared to increase the heat losses from the combustion chamber. In tests of an insulated piston in a diesel engine, Woschni et al. [83] observed increased heat transfer at higher temperatures. They proposed that the boundary layers were thinner for the hot TBC surfaces, leading to a drastic increase in the convective heat transfer coefficient. However, later investigations have instead attributed these problems to degraded combustion [3].

TBCs in the as-coated condition typically have much rougher surfaces than do steel pistons, which could be another reason for lower fuel efficiency than expected. For steel pistons, it has been demonstrated that a polished surface improves the fuel efficiency as the heat transfer area is reduced [84]. Wind tunnel tests of TBCs with varying degrees of surface roughness have found increased heat transfer for rougher surfaces [85]. When testing a metallic TBC on the piston of an SI engine, Marr et al. [86] found that the average heat flux was higher than for an uncoated surface, which was attributed to the greater surface roughness. When testing a metal-based TBC on the sparkplug of an SI engine, Marr et al. [87] found that heat transfer increased with surface roughness. Memme et al. [88, 89] demonstrated that, in an SI engine, polished coatings of metallic TBC or copper caused about a 3% improvement in fuel efficiency compared with the same coatings in as-sprayed condition. Because an increased heat transfer coefficient counteracts other benefits that can be obtained by using TBCs, surface roughness seems to be an important issue.

4 Methodology

In this chapter the methodology used for answering the research questions is presented. First, the various materials used in the studies are described. This is followed by the experimental methods used in determining the thermal properties, thermal cycling fatigue lifetime, optical properties, microstructure characterization, and mechanical properties.

4.1 Materials

4.1.1 TBCs for exhaust manifolds

Disc-shaped samples 12 mm in diameter were manufactured from a nodular cast iron, SiMo51, commonly used for exhaust manifolds. Also, test specimens shaped as screws, which later could be inserted into exhaust manifolds, were manufactured from SiMo51. The chemical composition of SiMo51 is 3.17C-4.15Si-0.40Mn-0.86Mo-0.10Cr-0.052Mg-Fe bal. (wt%).

Five different TBCs were fabricated using APS: YSZ with conventional microstructure, nanostructured YSZ having zones with partially unmelted small grains, lanthanum zirconate ($La_2Zr_2O_7$, LZ), mullite ($3Al_2O_3{\cdot}2SiO_2$), and forsterite ($2MgO{\cdot}SiO_2$) (see Table 1). The bond coat, Ni22Cr10Al1Y, was also applied using APS. These coatings were supplied by Oerlikon Metco (Wohlen, Switzerland).

Two sol-gel composite coatings were supplied by Datec Coating Corporation (Mississauga, Canada). A bond coat, Ni23Co20Cr8.5Al4Ta0.6Y, was first applied by plasma spraying. A silica sol-gel binder mixed with zirconia powder (4Ca1YSZ) was applied using two methods: spraying with an HVLP air gun (Binks model MG1; Carlisle Fluid Technologies, Scottsdale, AZ, USA) and dipping. After a layer was applied (9–11 µm for spraying, 8–10 µm for dipping), heat treatment was performed at 600°C for 30 min followed by 800°C for 10 min. This procedure was repeated until the coating consisted of ten layers.

Table 1: TBCs tested in exhaust manifolds.

TBC System	Bond coat	Top coat	Bond coat thickness [µm]	Top coat thickness [µm]
APS YSZ, conventional	NiCrAlY	8YSZ	135 ± 12	381 ± 13
APS YSZ, nanostructured	NiCrAlY	8YSZ Nano	135 ± 12	261 ± 23
APS LZ	NiCrAlY	$La_2Zr_2O_7$	135 ± 12	294 ± 7
APS, mullite	NiCrAlY	Mullite ($3Al_2O_3{\cdot}2SiO_2$)	135 ± 12	440 ± 21
APS, forsterite	NiCrAlY	Forsterite ($2MgO{\cdot}SiO_2$)	135 ± 12	301 ± 9
Sol-gel composite, sprayed	NiCoCrAlTaY	Sol-gel composite CaSZ/YSZ	50 ± 5	100 ± 10
Sol-gel composite, dipped	NiCoCrAlTaY	Sol-gel composite CaSZ/YSZ	50 ± 5	100 ± 10

4.1.2 YSZ TBCs for evaluation of lifetime, insulation, and mechanical properties

TBC samples with YSZ as the top coat were produced using APS by Oerlikon Metco (Wohlen, Switzerland) with a TriplexPro 210 spray gun (Oerlikon Metco), and using PS-PVD (University of Rzeszow, Poland) with a Metco O3CP (Oerlikon Metco) spray gun.

Fe24Cr8Al0.5Y (Amdry 9700) was used as the bond coat for all APS coatings, followed by a YSZ top coat with different types of microstructure (see Table 2). A top coat with conventional microstructure was produced from agglomerated and hollow spherical powder (HOSP) (Amdry 204NS-1) feedstock, a dense and segmented top coat from agglomerated and HOSP (Metco 204F) feedstock, and a nanostructured top coat from agglomerated and sintered (Metco 222A) feedstock.

A TBC with a columnar microstructure of the YSZ top coat was produced using the PS-PVD process. A low-pressure plasma spray (LPPS) process was used to deposit a NiCoCrAlY (Amdry 365-1) bond coat followed by agglomerated 7.5YSZ (Metco 6700) powder for the top coat in a PS-PVD process.

Three different metal films were deposited onto Amdry 204NS-1 samples on top of the ceramic (see Fig. 19). Silver and chromium layers were deposited onto the YSZ using a sputter coater (Q150T ES; Quorum Technologies, Lewes, UK), while Fe24Cr8Al0.5Y (FeCrAlY) was plasma-sprayed onto the ceramic.

Table 2: YSZ TBCs evaluated in the optical, thermal conductivity, and lifetime studies.

TBC System	Bond coat	Top coat	Bond coat thickness [µm]	Top coat thickness [µm]	Metallic top layer, thickness [µm]
APS, conventional	FeCrAlY	8YSZ Amdry 204 NS-1	94 ± 6	370 ± 4	-
APS, nanostructured	FeCrAlY	8YSZ Metco 222A	119 ± 4	353 ± 17	-
APS, segmentation cracks	FeCrAlY	8YSZ Metco 204F	137 ± 6	550 ± 16	-
APS, conventional + Ag layer	FeCrAlY	8YSZ Amdry 204 NS-1	123 ± 2	380 ± 16	Ag, 0.50
APS, conventional + Cr layer	FeCrAlY	8YSZ Amdry 204 NS-1	123 ± 2	380 ± 16	Cr, 0.15
APS, conventional + FeCrAlY layer	FeCrAlY	8YSZ Amdry 204 NS-1	89 ± 2	375 ± 18	FeCrAlY, 0–30
PS-PVD, columnar	NiCoCrAlY	7.5YSZ Metco 6700	83 ± 3	173 ± 16	-

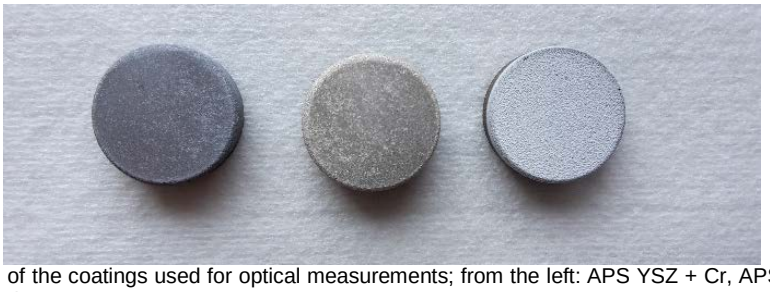

Figure 19: Three of the coatings used for optical measurements; from the left: APS YSZ + Cr, APS YSZ + Ag, and PS-PVD YSZ.

4.1.3 TBCs for in situ heat flux measurements

The circular sides of the heat flux probes facing the combustion chamber were coated with different APS TBCs by Oerlikon Metco (Wohlen, Switzerland) using an F4-MB-XL gun (Oerlikon Metco) with standard spray parameters. The FeCrAlY bond coat (Amdry 9700, Fe24Cr8Al0.5Y) was applied by plasma spraying onto heat flux probes manufactured from quenched and annealed 36CrNiMo6 steel.

Table 3: Analysed TBC materials in the in situ heat flux study. For all samples, the bond coat was Amdry 9700, FeCrAlY.

TBC system	Top coat	Top coat thickness [µm]	Bond coat thickness [µm]
APS YSZ, conventional	Amdry 204 NS-1	350 ± 10	82 ± 5
APS YSZ, sealed	Amdry 204 NS-1	340 ± 10	85 ± 3
APS YSZ, nanostructured	Metco 222A	330 ± 20	89 ± 4
APS YSZ, segmented	Metco 204F	280 ± 20	88 ± 8
APS LZ	$La_2Zr_2O_7$ XW0012	360 ± 10	82 ± 4
APS GZ	$Gd_2Zr_2O_7$ AE9768	410 ± 20	88 ± 7

A YSZ top coat with conventional microstructure and normal porosity was produced from agglomerated and HOSP (Amdry 204NS-1) feedstock (see Table 3). A dense YSZ top coat with segmentation cracks was produced from agglomerated and HOSP (Metco 204F) feedstock. A nanostructured YSZ top coat with nanozones was produced from agglomerated and sintered powder (Metco 222A). TBCs with lanthanum zirconate ($La_2Zr_20_7$, LZ) and gadolinium zirconate ($Gd_2Zr_20_7$, GZ) as top coats were produced from XW0012 and AE9768C powders, respectively. One heat flux probe with a conventional YSZ coating had the porosity sealed with aluminium phosphate.

4.2 Thermal properties

4.2.1 Laser flash analysis

The thermal diffusivity of the coatings was measured using laser flash analysis (LFA) equipment (LFA427; Netzsch, Selb, Germany) at Jönköping University. Steel specimens with a diameter of 12.8 mm and a thickness of about 1.5 mm, coated with TBC on one of the circular faces, were used for the LFA measurements. A thin layer of graphite was applied to the coated sample to maximize the amount of thermal energy absorbed by the surface during measurements. The thermal diffusivity measurements were performed at temperatures ranging from RT up to 800°C. The analysis software used a 3L heat loss + pulse correction model to calculate the thermal diffusivity of each layer.

In laser flash measurements, the coated side of the tested sample is heated by a pulse of energy from a laser and the temperature response on the reverse of the sample is measured. Thermal diffusivity, α, can then be determined as:

$$\alpha = 0.1388 \frac{L^2}{t(0.5)} \tag{6}$$

where L is the thickness of the sample and $t(0.5)$ is the time needed for the reverse of the sample to reach 50% of its maximum temperature [90]. The thermal conductivity, λ, is calculated as:

$$\lambda = \alpha \cdot C_p \cdot \rho \tag{7}$$

where α is the thermal diffusivity, C_p is the specific heat capacity, and ρ is the density. Literature data were used for the specific heat capacity while the density was calculated as:

$$\rho = (1 - \mathbf{f}) \cdot \boldsymbol{\rho_0} \tag{8}$$

where f is the fraction of pores in the coating and ρ_0 is the density of a pore-free specimen.

4.2.2 In situ heat flux measurements

A heat flux probe (see Fig. 20) that can be inserted into the combustion chamber of a heavy-duty diesel engine was developed in two master thesis projects [91, 92]. One intake valve was removed from a single-cylinder 2.1 dm^3 Scania diesel engine and was replaced with a stationary heat flux probe. The engine was thus running with only one intake valve and two exhaust valves working. The still functioning intake valve and valve seat were adjusted and tested in a gas flow test rig to ensure that the swirl number was the same as when two intake valves were being used.

The main parts of the heat flux probe are: (i) a support ring that is fastened with eight screws in the position of the valve seat; (ii) a semi-hollow shaft that is internally cooled with water or compressed air, has four thermocouples at different heights, and has a circular face where TBCs can be applied and exposed to gases in the combustion chamber; and (iii) a retainer that pushes the shaft against the support ring to prevent the leakage of combustion gases into the intake port. If the thermal conductivity, k, of the steel in the shaft is known, the heat flux through the TBC and up through the

shaft of cross-sectional area A can be calculated by measuring the temperature, T, at different heights, x. The heat flux, $\dot{q}$, can be calculated as:

$$\dot{q} = -kA \frac{\Delta T}{\Delta x} \tag{9}$$

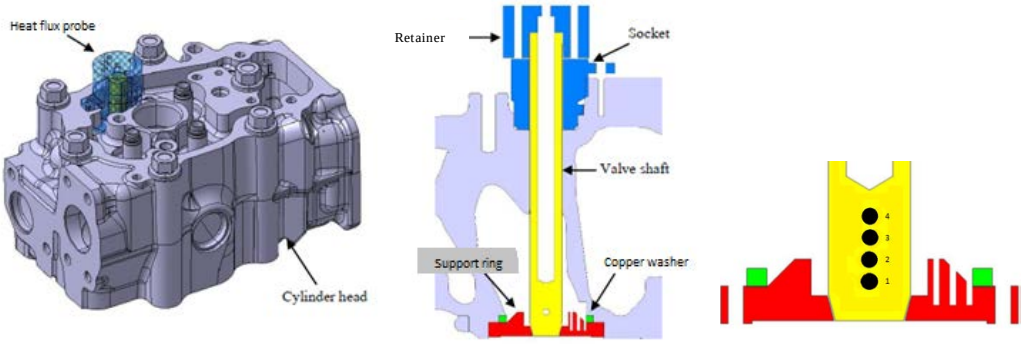

Figure 20: A heat flux measurement device positioned in one of the intake valves of a single-cylinder diesel engine. The coating to be tested is applied onto the lower surface of the shaft; adapted from Kianzad [92].

Efforts were made to ensure that the heat flux was as one dimensional as possible, i.e., that most of the heat flux through the tested TBC went up through the shaft and as little heat flux as possible went horizontally to/from the support ring or into the air surrounding the shaft within the intake port. Internal cooling of the shaft improved the heat flux in the vertical direction.

Thermocouples in the support ring were used in evaluating the temperature difference between the shaft and support ring at a certain distance from the combustion chamber. Insulating coatings of different thicknesses were tested on the lower face of the support ring. This was done to adjust the heat flux into the ring and, consequently, the temperature of the ring. The coating thickness that minimized the temperature difference between the ring and the shaft was used in all the actual heat flux tests.

The contact area between the shaft and ring was made conical, with slightly different angles for the two components to ensure that the contact area was small and situated at the lower end of the shaft. A small contact area minimized the potential heat flux between the two components, and a contact area near the combustion chamber prevented hot gases from leaking into the contact and heating the shaft from the side.

A copper washer was used to prevent leakage between the support ring and cylinder head. Gas leakage in that position would heat the shaft from the side and cause measurement errors. The intake port was blocked to prevent intake gas from entering the intake port and cooling the shaft from the side.

Typical temperatures at different distances from the combustion chamber are shown in Fig. 21. The heat flux results differed slightly depending on the position because of problems placing the thermocouples in the correct positions. The thermocouples were positioned in Ø3-mm holes drilled from the side to the centre of the shaft. X-ray analysis of the shafts showed that some thermocouples were not welded correctly on the lower side of the hole. This caused an error in the distance between the temperature measurements and in the heat flux calculations in Eq. 9. The thermocouples were acceptably positioned in two of the positions (2 and 4 in Fig .20), so only these two positions were used for the heat flux calculations.

The single-cylinder engine used for the test had a displacement of 2.1 dm^3; during the measurements, it operated at a constant 1200 rpm with 120 mg fuel/injection. Engine data and test parameters are shown in Table 4.

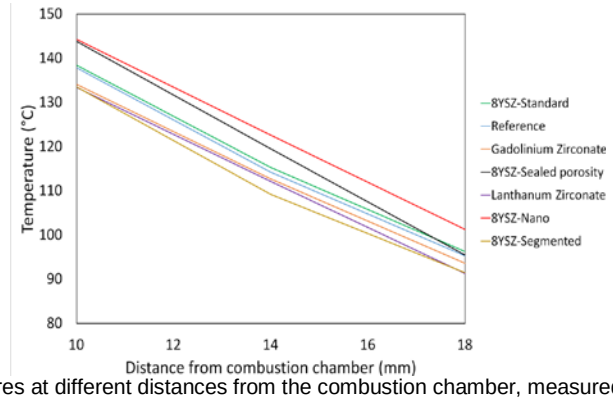

Figure 21: Temperatures at different distances from the combustion chamber, measured using the heat flux probe.

Table 4: Engine data and test parameters.

Engine test parameters	
Displacement	2.123 dm^3
No. of cylinders	1
Engine speed	1200 rpm
Bore/stroke	130/160 mm
Compression ratio	18.5:1
Load, short test	120 ± 0.6 mg /injection
Load, 5-h test	120 ± 1.0 mg/injection
Boost pressure	0.98 bar
Exhaust pressure	0.98 bar
Swirl number	1.7
Rail pressure	1200 bar
Start of injection (SOI)	–3°
Duration of heat flux test	3 × 15 min
Internal cooling of shaft for heat flux test	Water 24.8 ± 1.1°C, 0.90 l/min
Duration of running-in test	1 × 5 h
Internal cooling of shaft for running-in test	Compressed air: 7.7 bar pressure

4.3 Thermal cycling fatigue test/thermo-mechanical properties

The types of thermal cycling fatigue (TCF) faced by TBCs differ between the combustion chamber and the exhaust manifolds. In the combustion chamber, there is a combination of high cycle fatigue (HCF) and low cycle fatigue (LCF). The heating of the surfaces during combustion and the subsequent cooling of the surfaces in the ensuing following cycles causes the HCF of the coatings. The slower temperature variations due to factors such as the start/stop of the engine and variations in load give rise to LCF. In gas exchange components, such as exhaust manifolds and turbo manifolds, the TBCs are not exposed to any high temperatures from a flame, as in the combustion chamber. These components are mainly subjected to LCF.

4.3.1 TCF lifetime of TBCs for exhaust components, engine test

To evaluate the TCF of TBCs in exhaust manifolds, specimens shaped as screws were manufactured and coated with TBCs. The specimens were inserted into threaded holes (see Fig. 22), specially made for this purpose, to expose the TBCs to the exhaust gases. The coatings were then tested for 2000 h in a thermal cycling engine test (i.e., gas exchange test cycle) in which the exhaust gas reached temperatures up to 760°C (see Fig. 23). The TBCs could not be inspected during the test, but were analysed when removed after the full 2000-h test.

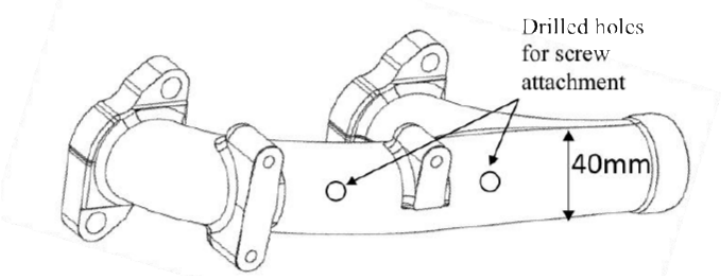

Figure 22: Exhaust manifold with threaded holes where TBC specimens can be placed and exposed to exhaust gases during an engine test [8].

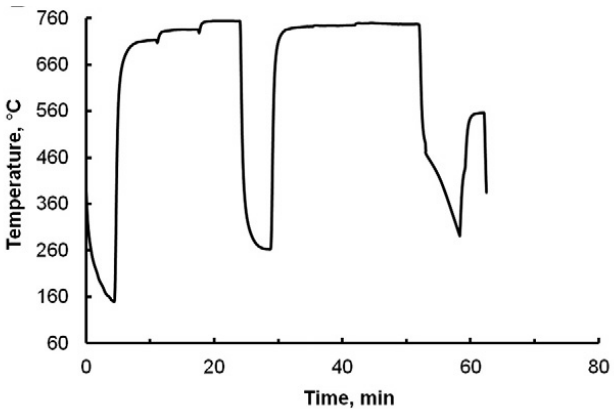

Figure 23: Exhaust gas temperature variations during an engine test cycle.

4.3.2 TCF lifetime of TBCs for exhaust components, furnace test

In addition to being subjected to TCF testing in an engine, the same types of TBCs were tested in a chamber furnace. The temperature was cycled between 180°C and 760°C, with a 15-min hold time at the maximum temperature. These temperatures were chosen to imitate the conditions in the gas exchange test cycle used in the tests with TBCs inserted into exhaust manifolds. The duration of each cycle was 140 min. Some of the samples were tested for 500 h while the rest were tested for 1000 h. The temperature profile is shown in Fig. 24.

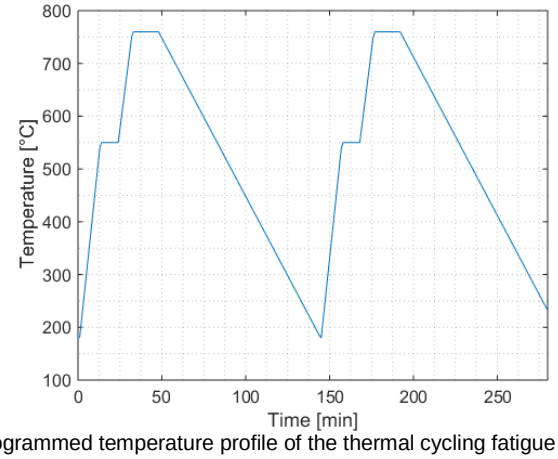

Figure 24: Programmed temperature profile of the thermal cycling fatigue test in a chamber furnace.

4.3.3 TCF furnace test

TCF tests using faster heating and cooling rates were conducted at Linköping University. Four TBC specimens at a time were positioned on a test table. During the heating stage, a furnace kept at 800°C was positioned over the specimens. The furnace was removed after 1 h, and the surface of the

TBC specimens was cooled for 320–370 s with compressed air until the temperature reached 100°C. The heating and cooling procedure was repeated 500 times. When visual inspection revealed spallation covering 20% or more of the surface, the specimen was removed. Fig. 25 shows the furnace and the temperature profile for the first three cycles of a TCF test.

In TCF tests, the growth of TGO is often a critical factor [93]. For NiCoCrAlY, which is commonly used as the bond coat in aerospace and industrial turbine applications, thermal cycling fatigue is often evaluated at temperatures up to 1100–1200°C [93–96]. The lower temperature (800°C) used in the current TCF test was chosen because of the particular conditions in diesel engines. The temperature of the bond coat is much lower, especially for components subject to forced cooling, such as the pistons and the cylinder heads. These lower temperatures also justify using bond coats with lower oxidation resistance, so FeCrAlY was used for some of the studied TBCs. Consequently, to imitate the conditions in a diesel engine and to avoid too-rapid TGO growth, the test temperatures need to be rather low.

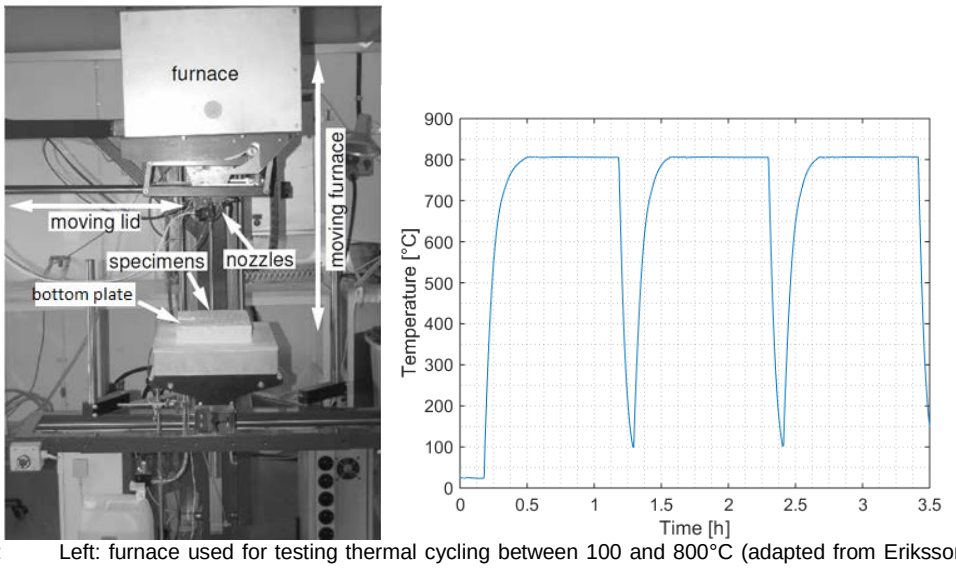

Figure 25: Left: furnace used for testing thermal cycling between 100 and 800°C (adapted from Eriksson [97]). Right: measured substrate temperature of the TBC samples in the LCF furnace test.

4.3.4 HCF engine test

In the in situ heat flux measurements described in section 4.2.2, probes were coated with TBCs and inserted into the combustion chamber of a single-cylinder diesel engine. After the 5-h heat flux test, the coatings were sectioned and the amount of damage due to the HCF exposure was analysed using a scanning electron microscope (SEM). The engine test lasted 5 h at an engine speed of 1200 rpm, which corresponds to 1.8×10^5 heating cycles.

4.4 Reflectance measurements

Reflectance measurements were performed at temperatures ranging from 20 to 700°C, using a Vertex 70 FTIR spectrometer (Bruker, Billerica, MA, USA).

The RT directional hemispherical reflectance (DHR) was measured using an integrated sphere at wavelengths of 1.25–33 µm. With the high-temperature, high-pressure cell used for measurements at elevated temperatures, DHR cannot be measured directly. Instead, the spectral specular reflectance, *R(T)*, was measured at temperatures ranging from 350 to 750°C in 50°C steps, as well as at RT, *R(RT)*. The directional hemispherical reflectance at high temperatures could then be calculated according to:

$$DHR(T) = DHR(RT) * \frac{R(T)}{R(RT)} \qquad (10)$$

4.5 Microscopy

An Axio light optical microscope (LOM) (Zeiss, Oberkochen, Germany) and a Sigma VP scanning electron microscope (SEM) (Zeiss) were used to acquire micrographs of the coatings. AxioVision image analysis software (Zeiss) was used to measure porosity and the area of hot-hardness indents in SEM and LOM images.

4.6 Tensile adhesive strength

Adhesive strength testing can be used in the quality control of received of TBC-coated samples, to evaluate whether they are worth testing further. It can also be used for samples tested in, for example, thermal cycling tests, to evaluate whether lateral cracks have started to propagate.

The tensile adhesive strength of TBCs was measured according to SS-EN 582. Test specimens 25 mm in diameter and 15 mm thick made of SiMo51 nodular cast iron were coated with TBCs. The reverse sides of the coated specimens were grit blasted, ultrasonically cleaned in ethanol, and finally rinsed with acetone. The specimens were then dried in a furnace for 3 h, as it was found that residual ethanol and acetone in the pores would otherwise influence the test results. The specimens were glued to steel bars using Ultrabond 100 (HTK Hamburg GmbH, Hamburg, Germany) and then cured at 180°C for 3 h. A Quasar tensile test machine (Galdabini, Cardano Al Campo VA, Italy) was used to test the adhesive strength of the coated specimens at a rate of 0.015 mm s^{-1}.

4.7 Hardness

RT Vickers hardness was measured on polished cross sections of the TBCs using micro-indentation hardness testing equipment (MXT30; Matsuzawa, Akita, Japan) with a 300-g load.

Hot hardness was measured using a Bofors hot-hardness tester, type 2, with an HV5 load. Hardness indents were made at temperatures ranging from 25 to 700°C. Due to the high load, and consequently large indents, the indents had to be made on the relatively large coated surfaces instead of the polished cross sections. A typical indent from the hot-hardness test is shown in Fig. 26.

SEM images of the hardness indents were measured in AxioVision image analysis software. The coated specimens had relatively rough surfaces, so the hardness indents were irregularly shaped. The conventional method of evaluating the indent size by measuring the diagonals was not applicable for these irregularly shaped indents, so the size was instead measured by determining the contours and using the image analysis software to calculate the projected area, A_{proj}, of each indent. Vickers hardness, *HV*, is normally evaluated as:

$$HV = 1.8544 \frac{F}{d^2} \tag{11}$$

where *d* is the average length of the diagonals and *F* is the applied force in kgf. When the projected area in the indents is measured, the hardness is instead evaluated as:

$$HV = 1.8544 \frac{F}{2 * A_{proj}} \tag{12}$$

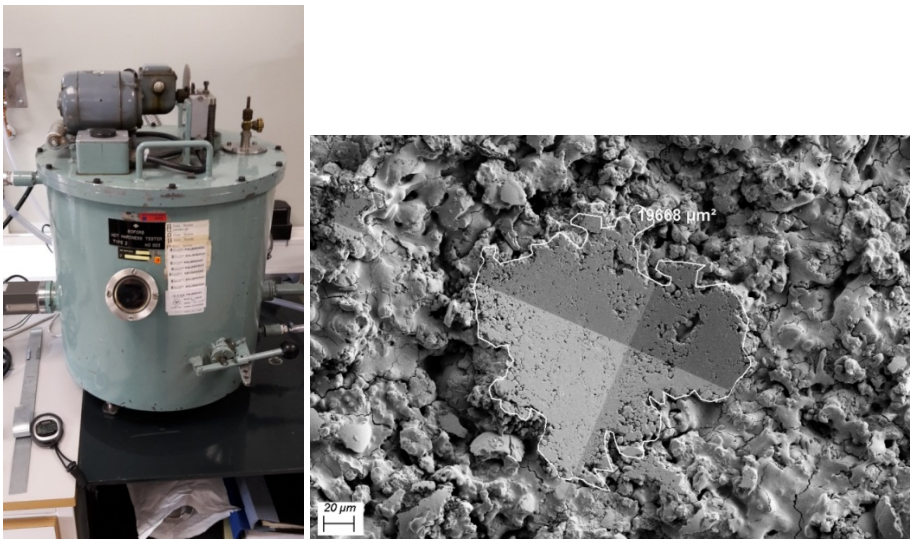

Figure 26: Hot hardness tester and an SEM image of an indent made at 500°C on the surface of a conventional APS YSZ coating. The boundaries of the indent were determined using image analysis software.

5 Results

5.1 Thermal cycling lifetime inside an exhaust manifold

The TCF test of TBCs inside an exhaust manifold as well as the TCF test in a chamber furnace indicated the best results for the plasma-sprayed nanostructured YSZ (see Table 5). There were no signs of spallation or an increased extent of microcracks.

Plasma-sprayed YSZ with conventional microstructure had an increased extent of microcracks. Small cracks that had formed adjacent to pores could be observed after the test, and surface cracks had also formed due to the thermal cycling. Both of these types of cracks were seen in each of the two TCF tests.

The $La_2Zr_2O_7$ TBC deposited by plasma spraying displayed surface cracks and an increased number of interlamellar cracks after both types of TCF tests. The surface cracks led to the spallation of micrometer-sized flakes after 1000 h of thermal cycling in the furnace.

Plasma-sprayed mullite displayed lateral cracks in the top coat/bond coat interface after furnace testing as well as some spallation at the edges. The top coat spalled off completely after the TCF test in the engine exhaust manifold. The plasma-sprayed forsterite had lateral cracks near the bond coat/top coat interface after both types of TCF tests. Fig. 27 shows the cracks and spallation for the mullite and forsterite coatings.

The sol-gel composite coatings were evaluated only in the furnace TCF test. Both coatings had an increased number of transversal cracks. The sprayed sol-gel composite coating displayed an increase in crack density from 5.3 mm^{-1} in the as-sprayed condition to 6.4 mm^{-1} after 500 h and 7.7 mm^{-1} after 1000 h. The dipped sol-gel composite coating had an original crack density of 5.6 mm^{-1}, which increased to 5.7 mm^{-1} after 500 h and 6.9 mm^{-1} after 1000 h.

Oxidation of the substrate under the bond coat was observed in all the plasma-sprayed TBCs after both types of thermal cycling. After the thermal cycling in air, the oxide scale consisted of Fe oxide, Fe-Si oxide, and Si oxide. The oxide scale after the thermal cycling in the exhaust manifold consisted only of Si oxide.

Table 5: Results of thermal cycling tests of TBCs for exhaust manifolds.

TBC	**Damage from thermal cycling in chamber furnace**	**Damage from thermal cycling in exhaust manifold**
APS YSZ, nanostructured	No test influence	
APS YSZ, conventional	Small cracks adjacent to pores; surface cracks	
APS, $La_2Zr_2O_7$	Increased number of interlamellar cracks; surface cracks; micrometer-sized spallation on the surface	
APS, mullite	Cracks along BC/TC interface; spallation on the edges	Complete spallation
APS, forsterite	Lateral cracks near bond coat	
Sol-gel composite, sprayed	Increased density of transverse cracks	Not tested
Sol-gel composite, dipped	Increased density of transverse cracks	Not tested

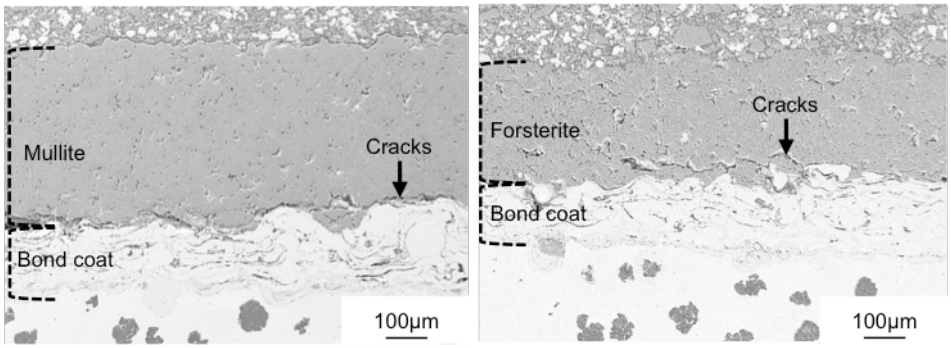

Figure 27: SEM images of the coating microstructure after thermal cycling in air for 1000 h showing (left) the mullite system and (right) the forsterite system.

5.2 Thermal modelling of TBCs on exhaust components

The RT thermal conductivity of the different TBCs evaluated in the TCF tests is presented in Table 6. The plasma-sprayed conventional YSZ and $La_2Zr_2O_7$ TBCs had the lowest values, 0.7 Wm^{-1} K^{-1} and 0.8 Wm^{-1} K^{-1}, respectively. Surprisingly, the nanostructured YSZ coating had a higher thermal conductivity, 1.3 Wm^{-1} K^{-1}, than did the conventional YSZ coating, even though the nanozones could be expected to contribute to phonon scattering and decreased thermal conductivity. The coatings with the highest thermal conductivity were the mullite (2.7 Wm^{-1} K^{-1}) and sol-gel composite (8.2 Wm^{-1} K^{-1}) coatings. No reliable data were obtained for forsterite.

The temperature decrease beneath TBC layers of different thicknesses and thermal conductivities inside a straight pipe was calculated according to a method presented elsewhere [59]. A temperature decrease of 50°C in the metallic substrate is required to extend the lifetime of exhaust components [98, 99]. As can be seen in Fig. 28, a top coat thickness of 1.3 mm is needed for a plasma-sprayed conventional YSZ TBC with a thermal conductivity of 0.7 Wm^{-1} K^{-1} to achieve a 50°C decrease in temperature. For mullite, with a thermal conductivity of 2.7 Wm^{-1} K^{-1}, a top coat more than 5 mm thick would be required.

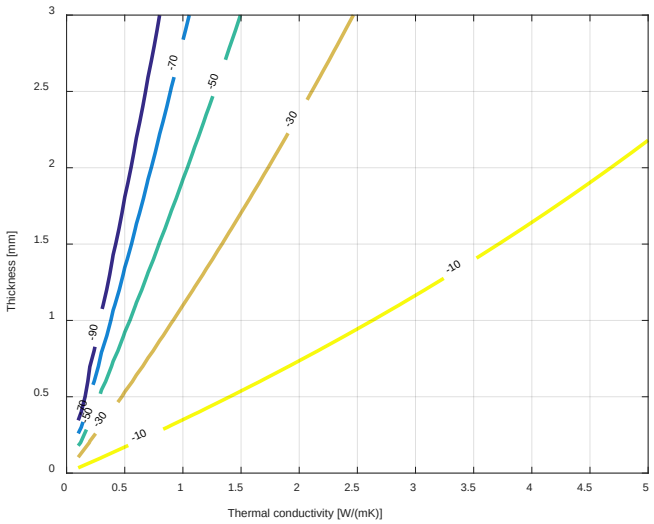

Figure 28: Temperature decrease beneath TBCs of different thicknesses and thermal conductivities when the exhaust gas temperature is 760°C; adapted from Ekström et al. [59].

Table 6: Coefficient of thermal expansion (α) [100, 101], density (ρ), density of pore-free material (ρ_0) [102–105], specific heat (C_p), and thermal conductivity (λ) [20, 100].

	Mullite	Forsterite	8YSZ	YSZ Nano	$La_2Zr_2O_7$	Sol-gel composite sprayed
α, $K^{-1} \cdot 10^{-6}$	5.3	9.5	10.7	11.0	9.1	...
ρ_0, g cm^{-3}	3.16	3.27	6.10	6.10	6.05	...
ρ, g cm^{-3}	2.68	2.59	5.12	4.62	5.01	3.90[a]
C_p, J $(g \cdot K)^{-1}$	0.76	0.84	0.46	0.46	0.39	0.66[a]
λ, W $(m \cdot K)^{-1}$ [b]	2.7 ± 0.3	...	0.7 ± 0.05	1.3 ± 0.05	0.8 ± 0.06	8.2[a]
λ, W $(m \cdot K)^{-1}$ [c]	3.3	5.0	1.2	1.1	1.6	...

[a] Data provided by Datec Coating Corporation
[b] Measured at RT
[c] Literature data at RT

5.3 Thermal cycling lifetime

The thermal cycling lifetime of four YSZ coatings with different types of microstructure is shown in Fig. 29, while Fig. 30 shows the appearance of the samples after the test. APS-coated specimens with nanostructured and conventional microstructures all failed before 85 cycles. APS-coated specimens with segmented microstructure lasted much longer, 350–450 cycles, due to the higher strain tolerance provided by the vertical cracks. The FeCrAlY bond coat used with these APS coatings was severely oxidized. The TGO was 25 µm thick for the conventional APS coating, 30 µm for the nanostructured coating, and 90 µm for the segmented coating (see Fig. 31). The bond coat temperature must therefore be lower than the temperature during the TCF test (800°C) for FeCrAlY to be a viable alternative. The APS coatings partly failed in both the TGO and YSZ layers.

The PS-PVD specimens with a NiCoCrAlY bond coat lasted 500 cycles without any signs of spallation. The combined effects of a more oxidation-resistant bond coat, a thinner top coat, and high strain tolerance due to the columnar microstructure explain the excellent results. The TGO thickness was only about 1.5 µm.

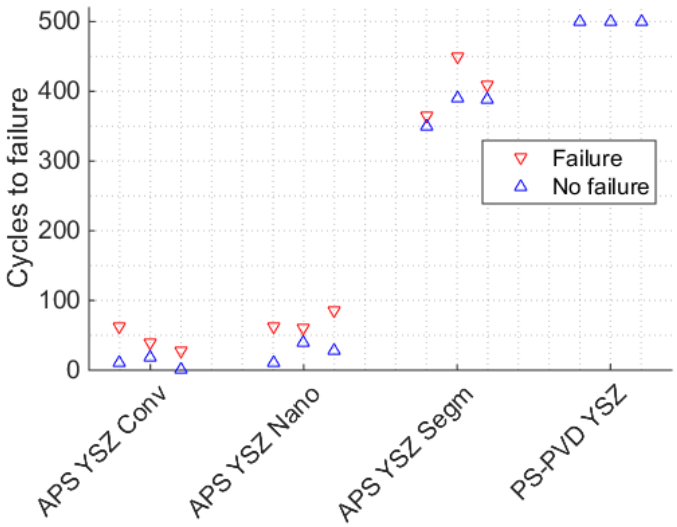

Figure 29: Thermal cycling results for four different YSZ coatings. Coating failure occurred in the interval between the blue and red triangles.

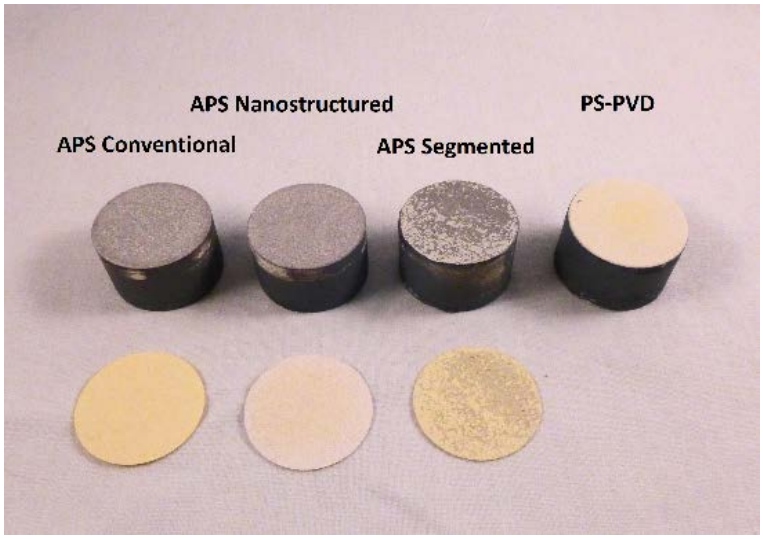

Figure 30: Specimens after thermal cycling. The entire top coat has spalled off the three APS coatings.

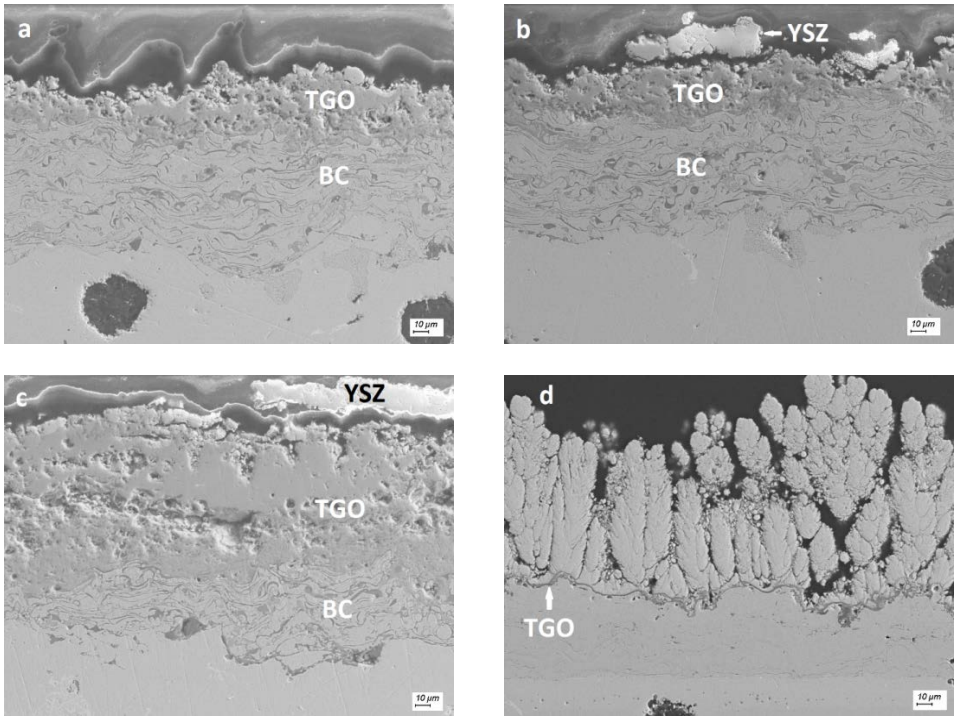

Figure 31: SEM images of cross sections of TCF samples: (A) conventional APS YSZ with 25-µm TGO, (B) nanostructured APS YSZ with a 30-µm TGO, (C) segmented APS YSZ with a 90-µm TGO, and (D) PS-PVD YSZ with a 1.5-µm TGO. The APS coatings failed partly in the TGO and partly in the YSZ, while the PS-PVD was intact after the TCF test.

5.4 Thermal insulation properties

In a combustion chamber in a heavy-duty diesel engine, it can be argued that both the thermal conductivity and the reflectance influence how effectively a TBC can reduce the heat flux. The RT reflectance of YSZ TBCs, with different types of microstructures and with three different metallic coatings on top of the ceramic, is shown in Fig. 32. The temperature dependence of the reflectance at a selected wavelength, 2 µm, is shown in Fig. 33. It is apparent that the type of microstructure greatly influences the reflectance of YSZ TBCs. Nanostructured and conventional microstructures had higher reflectance than did segmented TBC. A PS-PVD coating with a columnar microstructure had a relatively poor reflectance at low temperature, but an increasing reflectance with temperature,

and was the coating with highest reflectance at temperatures above 650°C. The increase in reflectance with temperature was probably related to oxygen diffusing into the coating and reducing the number of oxygen vacancies in the ceramic. Fewer oxygen vacancies lead to lower absorbance and consequently higher reflectance.

The metallic coatings (i.e., Ag, Cr, and FeCrAlY) had relatively low reflectance at the short wavelengths that are most important in a diesel engine. However, the silver coating had slightly higher reflectance than did the segmented YSZ TBC.

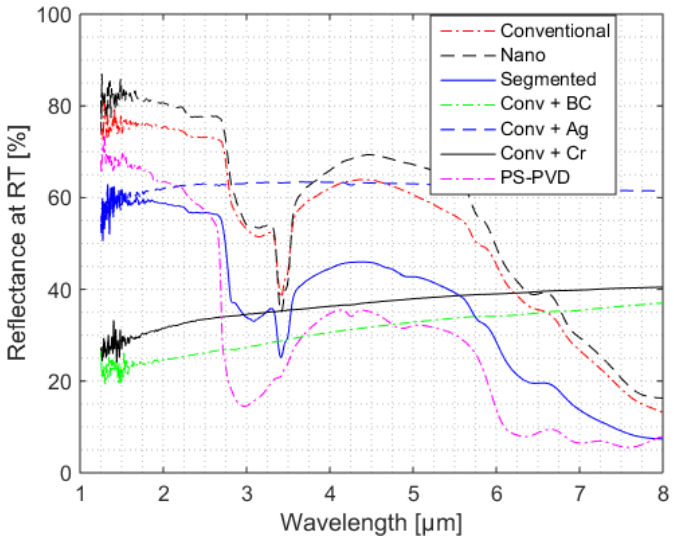

Figure 32: Room temperature reflectance of evaluated TBCs.

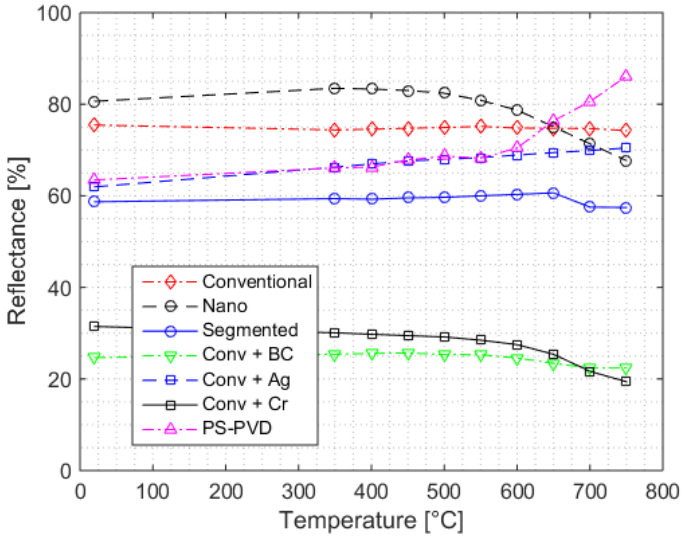

Figure 33: Reflectance at 2.0-µm wavelength at elevated temperatures.

The thermal conductivities of various APS microstructures are shown in Fig. 34. The coatings with nanostructured and conventional microstructures had the lowest thermal conductivities, while the thermal conductivity of the segmented coating was over twice as high over the entire temperature range.

The conventional and nanostructured TBCs had the lowest thermal conductivities as well as the highest reflectance at temperatures up to 600°C, indicating that these types of microstructures have the highest potential for thermal insulation.

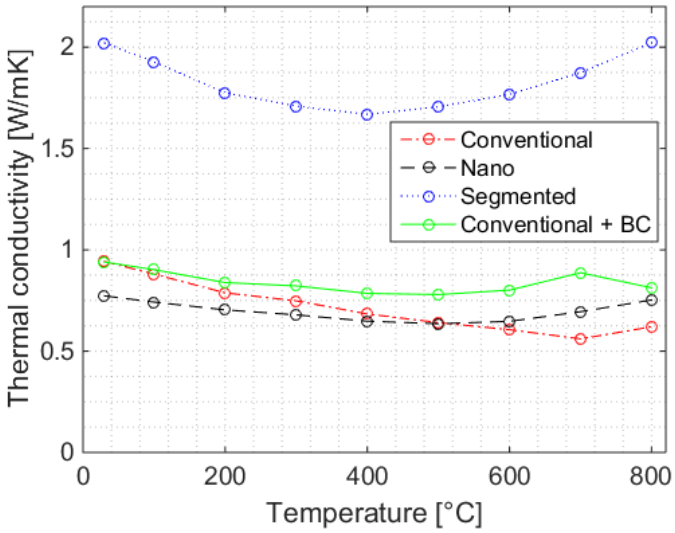

Figure 34: Thermal conductivity of APS TBCs.

5.5 Heat flux reduction from the combustion chamber

The normalized heat flux with and without TBC on a probe measuring the heat flux through the combustion chamber wall is shown in Fig. 35. YSZ coatings with different types of microstructure (i.e., conventional, nanostructured, and segmented) reduced the flux by 0.2–1.8% versus that of an uncoated steel reference. A top coat consisting of $La_2Zr_2O_7$ was about as effective as was conventional YSZ in reducing the heat flux. $Gd_2Zr_2O_7$ was the most efficient TBC, probably due to a combination of low thermal conductivity and high reflectance, and reduced the heat flux by 4.7%. Sealing the pores of the conventional YSZ coating with aluminium phosphate resulted in higher heat fluxes than that of the steel reference, possibly due to the decreased reflectance of the coating and consequently increased radiative heat transfer through it.

The surface roughness of the various coatings was measured, as this factor can influence the heat transfer (see Table 7). The segmented YSZ coating had the lowest Ra value, while the conventional and nanostructured YSZ coatings had the highest Ra values.

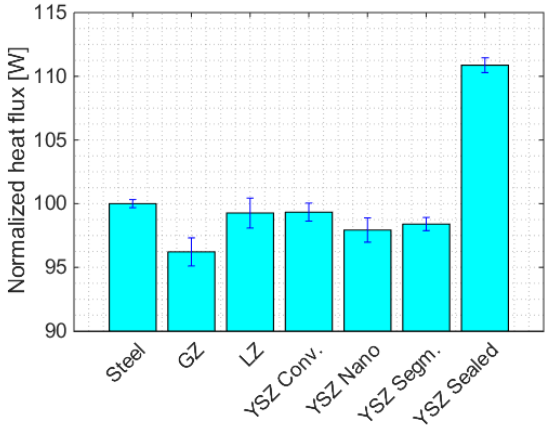

Figure 35: Normalized initial heat flux values after correction for varying heat loads.

Table 7: Surface roughness parameters of coatings in as-sprayed condition.

TBC system	Rz [µm]	Ra [µm]	Rk [µm]	Rpk [µm]	Rvk [µm]	MR1 [%]	MR2 [%]
Conventional YSZ	65.7	11.2	34.3	21.8	16.6	13.1	89.7
Sealed YSZ	34.0	5.5	16.2	4.1	18.2	8.1	85.0
Nano YSZ	60.8	10.8	38.4	16.8	15.8	12.9	92.8
Segmented YSZ	24.0	4.0	13.7	6.8	5.9	12.0	90.7
LZ	38.8	5.6	17.0	9.5	11.5	12.3	88.4
GZ	38.5	6.3	22.5	15.8	6.7	13.5	92.4

5.6 Running-in of TBCs inside the combustion chamber

The running-in behaviour, in terms of heat flux, of the various top coat materials is shown in Fig. 36. The insulation properties of a top coat consisting of plasma-sprayed YSZ with conventional microstructure improved over time. This was attributed to the growth of microcracks, perpendicular to the direction of the heat flux, near the bond coat, as shown in Fig. 37. Also, $Gd_2Zr_2O_7$ had improved thermal insulation properties over time, but this was due to the growth of a large crack in the top coat. Continued exposure to the combustion chamber would soon have resulted in the spallation of much of the top coat. The $La_2Zr_2O_7$ did not display any positive running-in behaviour. The running-in time for the YSZ as well as for $Gd_2Zr_2O_7$ was about 3 h.

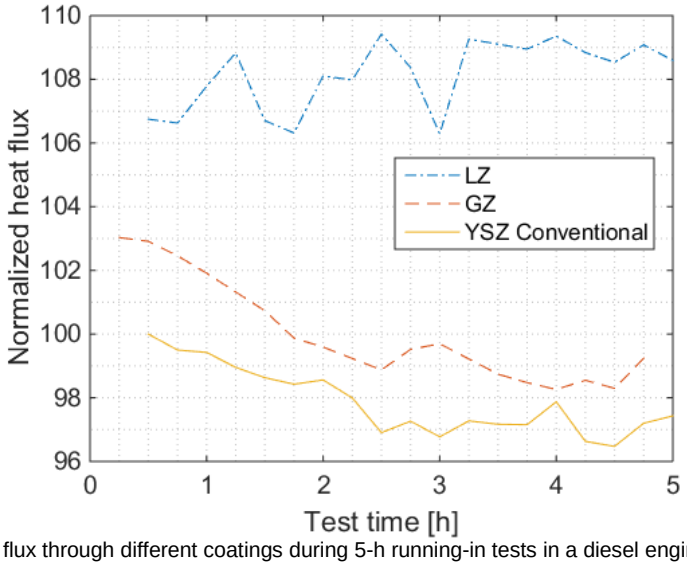

Figure 36: Heat flux through different coatings during 5-h running-in tests in a diesel engine.

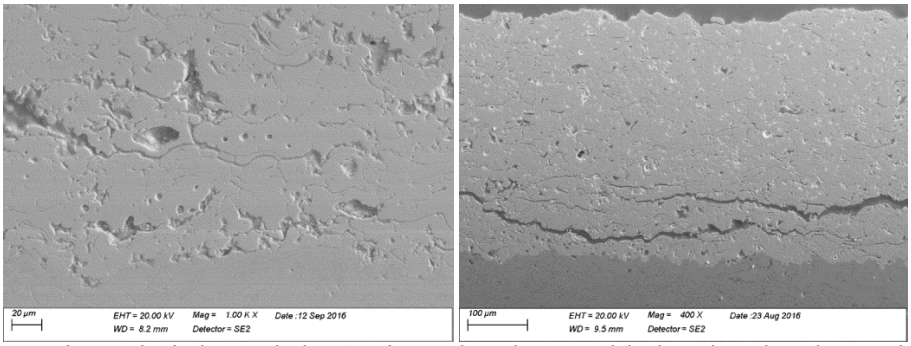

Figure 37: Left: growth of microcracks in YSZ after a 5-h engine test. Right: large lateral cracks near the bond coat in the GZ coating after a 5-h test.

6 Discussion, conclusions, and future work

6.1 Discussion

6.1.1 What is the thermal cycling performance and crack behaviour of different TBCs for exhaust manifold applications?

The conditions in exhaust components differ from those inside the combustion chamber in certain important respects that influence the thermal cycling lifetime. In exhaust components there is:

1. no high cycling fatigue from combustion events
2. lower gas pressure and lower-pressure pulsation
3. considerably higher bond coat temperature due to the absence of active cooling of the substrate
4. higher top coat temperature

The first two factors positively influence the thermal cycling lifetime of TBCs inside exhaust components versus inside the combustion chamber. The absence of HCF reduces the risk of surface cracks in the TBC. As has been demonstrated by Miller and Zhu [106], the combined effect of LCF and HCF is worse than that of LCF alone. The lower gas pressure and lower-pressure pulsations in the exhaust stream than inside the combustion chamber lead to lower mechanical load on the TBCs.

The higher bond coat temperatures in exhaust components increase the growth rates of TGO. These temperatures and growth rates, however, are still very low compared with those in gas turbine applications, where TGO thickness often limits the lifetime of the TBCs. For bond coats with high oxidation resistance, such as NiCrAlY or NiCoCrAlY alloys, the TGO thickness may not be a problem. On bond coats exposed in exhaust manifolds, the TGO layer was very thin. For FeCrAlY bond coats, having much higher oxidation rates, as seen in the TCF test presented in Paper B, the high bond coat temperatures lead to thick TGO layers that will likely limit the lifetime of the TBC. Oxidation of the substrate beneath the bond coat was observed for the plasma-sprayed TBCs after thermal cycling. This indicates that oxygen transport was not halted by the bond coat, and that oxygen was able to reach the substrate. A less porous bond coat would be preferred in order to protect the substrate from oxidation.

Thermal stresses in the top coat are dependent on the temperature range during thermal cycling. The higher TBC surface temperatures in exhaust components will lead to higher thermal cycling stresses than in combustion chamber components. These stresses likely caused the large lateral cracks in the forsterite and mullite TBCs and the smaller cracks in the YSZ and $La_2Zr_2O_7$ TBCs found in the TCF test presented in Paper A.

6.1.2 How is the substrate temperature of exhaust components influenced by different TBCs and different coating thicknesses?

A lower cast iron temperature would prolong the lifetime of the exhaust and turbo manifolds, due to a lower oxidation rate and improved fatigue resistance. A 50°C decrease in the temperature of the metal beneath the TBC would be desirable, based on the results of earlier studies [98, 99]. The sol-gel composite coatings had promising TCF lifetimes. However, the high thermal conductivity (about 8.2 W^{-1} K^{-1}) of these TBCs makes them difficult to use for exhaust components. A top coat over 15 mm thick would be required to achieve the required 50°C decrease in substrate temperature. Such thick coatings lead to several different problems. Coating processes often lead to residual stresses in the TBCs, which may lead to premature cracking. The coatings may also be very expensive, due to the multiple layers required to build the required thickness and to the material cost of such thick coatings. The increased outer dimensions needed to compensate for thick coatings and the resulting increased component weight are also factors that limit the acceptable coating thickness.

A better solution would be to use TBCs with much lower thermal conductivities so that the TBCs do not have to be as thick. TBCs with thermal conductivities of 0.7–0.8 W^{-1} K^{-1} can be manufactured

by plasma spraying, with YSZ or LZ as the top coat. A top coat about 1.3–1.5 mm thick would be required to achieve a 50°C temperature decrease in the substrate of such TBCs. However, even lower thermal conductivities would be preferred, so the thickness could be reduced even further.

As atmospheric plasma spraying is a line-of-sight process, it cannot be used to coat the entire inner surface of long, narrow pipes. However, by spraying from the ends of a pipe, a TBC can be applied a few cm into the pipe. Because some exhaust components have the highest thermal loads near their ends, coating even these small portions of the components may be enough for a significant improvement in fatigue lifetime. If a TBC is required farther inside the pipe, a coating process such as a slurry or sol-gel process would be better.

6.1.3 How do different coating microstructures, produced using APS and PS-PVD, influence the thermal cycling lifetime of the TBC?

The type of microstructure greatly affects the thermal cycling lifetime of the TBC. APS coatings with segmented microstructure outperform the conventional and nanostructured YSZ APS coatings by a factor of 5–10. The columnar microstructure of the PS-PVD coating survived the TCF test even longer, but the better oxidation resistance of the bond coat and lower thickness of the top coat made it difficult to make a fair comparison with the APS coatings. However, it can be concluded that the high strain tolerance caused by the cracks perpendicular to the substrate in the segmented APS coating, and by the gaps between the columnar grains in the PS-PVD coating, has a positive effect on the thermal cycling lifetime. This supports the findings of others who have observed long thermal cycling lifetimes for APS coatings with segmentation cracks [13, 27] and for PS-PVD coatings with intercolumnar gaps [30, 31]. The influence of nanozones on thermal cycling lifetime was found to be negligible, in contrast to the findings of others [20, 21].

The severe oxidation of the FeCrAlY bond coat in the TCF test with 800°C as the maximum temperature indicates that a bond coat with higher oxidation resistance is needed at such temperatures. The bond coat used on exhaust components, such as exhaust and turbo manifolds, can reach temperatures exceeding 700°C. Bond coats in which iron has been replaced with nickel or nickel/cobalt would be better for these components due to their improved high-temperature oxidation resistance. However, oxidation rates of FeCrAlY have been found to be rather low at temperatures up to 600°C [60]. For combustion chamber components with active cooling, such as the piston and cylinder head, FeCrAlY is expected to perform well as the bond coat.

The different types of microstructure are likely to spall in different ways once they fail. The PS-PVD coating with its columnar structure, with weak or no bonding between the individual columnar grains, is likely to fracture into smaller fragments before reaching the turbocharger. The associated risk of damage to the turbine wheel blades is therefore lower for the columnar than the other investigated types of microstructure.

6.1.4 How do different coating microstructures, produced using APS and PS-PVD, influence the thermal insulation properties of the TBC?

For exhaust components, where the TBC is not exposed to thermal radiation from a high-temperature flame, optical properties are not as important as they are inside the combustion chamber. The temperature gradients from the gas to the substrate are relatively small, due to the lack of forced cooling of the substrate. The thermal radiation from the exhaust gas towards the bond coat can be expected to be almost balanced by the thermal radiation from the bond coat towards the gas, due to the relatively small temperature difference between them. Thermal insulation in exhaust components is thus mainly determined by the thermal conductivity of the top coat.

Thermal radiation is more important for the thermal insulation for TBCs on combustion chamber components than for exhaust components. This is due to thermal radiation from the flame and to greater temperature differences between the gas and the bond coat as well as between the top coat surface and the bond coat. Thermal insulation of the TBC is therefore dependent on the combined thermal conductivity and optical properties of the TBC. The importance of the optical properties inside the combustion chamber also varies between engines, due to factors such as the amount of exhaust gas recirculated into the engine, compression ratio, load, and fuel.

The conventional and nanostructured APS TBCs had the lowest thermal conductivities – less than half those of the segmented APS coating and slightly lower than the literature data on PS-PVD coatings [31, 32]. Conventional and nanostructured APS coatings therefore have the types of microstructure that provide the best thermal insulation inside exhaust components and in combustion chambers where the thermal radiation is of only minor importance. The high reflectance of nanostructured APS coatings at low and moderate temperatures and of PS-PVD coatings at high temperatures, together with their low thermal conductivities, positions them as the preferred alternatives in engines where the influence of thermal radiation is significant.

The RT reflectance of the approximately 0.4-mm-thick conventional and nanostructured YSZ coatings was about 75–85% at wavelengths below 3 µm. Similar values have been reported by Eldridge et al. [70] for APS YSZ coatings. They measured coatings 0.125 and 0.68 mm thick, which had reflectance values of 60–70% and more than 90%, respectively. Thicker coatings have higher volume scattering and higher reflectance values than do thinner coatings. The larger numbers of scattering defects, such as grain boundaries, pores, and cracks, in the nanostructured YSZ coating than in the conventional coating explain its slightly higher reflectance. The low reflectance of the segmented coating, despite being the thickest one, can be attributed to its dense microstructure with few scattering defects. The relatively low reflectance of the PS-PVD coating is because it is less thick than the other coatings, and because of the fewer pores and grain boundaries associated with this coating process.

High-temperature reflectance measurements revealed decreasing reflectance with temperature for the nanostructured coating, possibly due to sintering that reduces the number of scattering defects in the coating. The PS-PVD coating had increasing reflectance at elevated temperatures at the investigated 2-µm wavelength and was the coating with the highest reflectance above 650°C. This increase in reflectance is probably due to oxygen diffusing into the coating and reducing the number of oxygen vacancies formed during spraying. Oxygen vacancies can easily form due to the reducing conditions in the low-pressure plasma plume in the PS-PVD process [30]. Stuke et al. [107] demonstrated that annealing an APS YSZ coating at 600°C for 1 h increases its reflectance due to the decreased number of oxygen vacancies and resulting decrease in the absorbance. The reflectance of a PS-PVD coating can thus be increased by annealing. Alternatively, the number of oxygen vacancies can be reduced during spraying by increasing the oxygen flow to counteract the reducing conditions [30], which would increase the reflectance.

The reflectance of a conventional YSZ coating with a silver layer on top of the ceramic was relatively low. Of the ceramic coatings, only the segmented YSZ coating had lower reflectance than the silver coated TBC. By polishing the YSZ coating to a smoother surface before applying the silver layer, and by ensuring that the silver deposition process produces a smooth surface, the reflectance could be enhanced still further. The silver coating was not tested in an engine, however, and there is a risk that its reflectance will not remain stable over time in that environment.

6.1.5 How is the heat flux from the combustion chamber influenced by TBCs with respect to their composition, microstructure, and sealed porosity?

The heat flux probe measures the combined effect of thermal transport by conduction and radiation through the TBC. As compared with an uncoated steel reference sample, the heat flux was reduced by 4.7% with a GZ coating, 0.9% with a conventional YSZ coating, and 0.6% with an LZ coating. Of these coating materials, dense GZ and LZ both have about 25% lower thermal conductivities than does dense YSZ [43]. The heat flux reductions can therefore not be fully correlated to the thermal conductivity of the coatings, as optical properties must also be considered. GZ has lower transmittance and higher reflectance than does YSZ at wavelengths below 2.7 µm [77], which, together with its low thermal conductivity, explains why it provides better thermal insulation. The slightly greater thickness of the GZ coating, 410 µm versus 350 and 360 µm for YSZ and LZ coatings, respectively, is another important factor that contributes to the heat flux reduction.

The three YSZ coatings with different microstructures all produced rather small reductions in heat flux from the combustion chamber. The heat flux reduction was 1.8% for the segmented coating compared with 0.2% and 0.9% for the nanostructured and conventional coatings, respectively. The

fact that the segmented coating produced the largest heat flux reduction, despite having the highest thermal conductivity and lowest reflectance of the three, indicates that additional factors influence the heat transfer through the coatings. One factor may be the very low porosity of the segmented coating, which means that a small amount of hot gas can penetrate into the coating and heat it at some depth below the surface. The segmented coating also has the lowest surface roughness, contributing to lower heat losses, as others have demonstrated for similar surfaces [84–89]. The very small extent of nanozones – only about 0.2 area% – in the nanostructured YSZ coating explains why the heat flux result is about the same as for the conventional YSZ coating. Nanostructured coatings with more nanozones can be expected to be better at reducing the heat flux, as nanozones have been demonstrated to reduce the thermal conductivity [19] and a decreased pore size reduces the radiative heat transfer [108].

The conventional YSZ with the pores sealed with aluminium phosphate had a significant increase in heat flux, even though the thermal conductivity of the sealed coating can be expected to be much lower than that of steel. Increased radiative heat transport, because of the sealed pores, is believed to be the main reason for this high heat flux. Infiltrating pores in YSZ coatings with epoxy (refractive index n = 1.66) or CMAS (n = 1.62) has been demonstrated to reduce the scattering coefficient, and consequently also the reflectance, with a large increase in thermal radiation transmitted though the coating as a result [109, 110]. Filling the pores with aluminium phosphate (n = 1.51 [111]) may have a similar effect. When the pores are filled with a substance with a higher refractive index than that of air (n = 1.00), the scattering will decrease. The reflectance of the coating decreases and more thermal radiation will penetrate into the coating and cause deep heating. Sealing the pores may therefore cause more problems than it solves. Having a sealing substance with a low refractive index might reduce the problems of low scattering.

6.1.6 Is there a running-in period, with respect to thermal insulation properties, for TBCs inside a combustion chamber?

High-temperature exposure may result in changes in thermal conductivity over time due to sintering or the growth of microcracks [67, 68]. The effect decreases over time until a more steady-state thermal conductivity value is reached. Plasma-sprayed GZ coatings as well as YSZ coatings with conventional microstructure both had a running-in period of about 2–3 h before a more stable heat flux value was reached. For YSZ coatings, the heat flux through the TBC decreased over time. Microstructural analysis indicated that interlamellar cracks near the bond coat had increased in length. Because these cracks are oriented perpendicular to the heat flux, they are effective in improving the thermal insulation. For the GZ TBC there was also a reduction in heat flux, but due to the growth of a large lateral crack near the top coat/bond coat interface. The orientation of this crack was also effective in reducing the heat flux, as with the interlamellar cracks in the YSZ coating. However, the size of the crack suggests that the coating was close to spalling.

Unlike the other two TBCs, the LZ coating had no running-in period. A large crack, oriented mainly in the lateral direction, was found in the LZ coating after the 5-h test. It is reasonable to believe that a crack of that size and orientation would result in a similar decrease in heat flux as that produced by the crack in the GZ coating if it had formed during the test. The crack may have either existed in the coating before the test or, more likely, formed after the test.

6.1.7 How can the results be used?

The results indicate that the bond coat oxidation is low for exhaust components in heavy-duty diesel engines, but that the substrate is sensitive to oxygen transport through the TBC. When designing a TBC to be used inside exhaust components, it is important to ensure low oxygen transport through the bond coat, for example, by reducing the porosity or changing the chemical composition.

The results of the thermal cycling tests of TBCs for exhaust components indicated a large spread in the extent of cracks in the top coats, ranging from no influence at all to complete spallation. The thermal conductivity measurements and the calculated temperature decreases in the substrates of these coatings also indicated large differences between the materials. These results give guidance as to what TBC to use inside an exhaust manifold, depending on the lifetime and thermal insulation requirements.

The heat flux through a TBC inside a combustion chamber is influenced not only by the thermal conductivity of the TBC, but also by factors such as the optical properties of the coating, surface roughness, hot gas leaking into the coating through pores, and the presence of soot on the surface. The in situ heat flux results indicate the true insulation properties of some TBCs under one set of operating conditions. This measurement technique, which was developed here, can be used for further studies of how various coating modifications can further improve the thermal insulation properties.

It is also important to remember the limitations of some of the coating processes. The PS-PVD coating process performs well in many ways. However, the coating thickness that can be produced with this process is limited, and not all substrates can be used due to the relatively high substrate temperature during this coating process.

Line-of-sight processes, such as APS, can only coat surfaces that are in a direct line from the spray gun. These coating processes can also have limitations in terms of the usable spray angle between the gun and the substrate. This causes problems for components with complex geometries. For example, APS can only coat a small part of the inner surface of a narrow pipe closest to its ends.

6.2 Conclusions

What is the thermal cycling performance and crack behaviour of different TBCs for exhaust manifold applications?

Plasma-sprayed nanostructured YSZ coatings displayed the best performance in the TCF test in the engine, showing no signs of damage. Plasma-sprayed top coats consisting of YSZ with conventional microstructure and $La_2Zr_2O_7$ also had promising thermal cycling lifetimes. These two coatings displayed some surface cracks and a small increase in the number and length of interlamellar cracks after the TCF test. For plasma-sprayed forsterite, the TCF test resulted in an increased number of cracks in the top coat as well as the growth of lateral cracks near the bond coat. The mullite top coat, also produced using plasma spraying, was completely spalled off. Sol-gel coatings, which were subjected only to TCF testing and were not tested in an engine, survived the thermal cycling without spallation.

How is the substrate temperature of exhaust components influenced by different TBCs and different coating thicknesses?

For a top coat thickness of 0.2 mm, the thermal conductivity needs to be as low as 0.1 $Wm^{-1}\,K^{-1}$ to achieve the required temperature decrease. A more normal thermal conductivity value is about 1.5 $Wm^{-1}\,K^{-1}$; in that case, the top coat would need to be 3 mm thick to reduce the substrate temperature by 50°C.

How do different coating microstructures, produced using APS and PS-PVD, influence the thermal cycling lifetime of the TBC?

Microstructures with high strain tolerance performed the best in the TCF test designed for testing TBCs under conditions similar to those encountered in a heavy-duty diesel engine. The segmented APS coating, with high strain tolerance due to the vertical cracks, survived 5–10 times more cycles in the TCF test than did either conventional or nanostructured APS coatings. The columnar microstructure produced using the PS-PVD process, with high strain tolerance due to the gaps between the columns, performed the best of all coatings in the TCF test.

How do different coating microstructures, produced using APS and PS-PVD, influence the thermal insulation properties of the TBC?

The coating microstructure with the best thermal insulation properties, here defined as a combination of low thermal conductivity and high reflectance, was the nanostructured APS coating, followed by the conventional APS coating, at temperatures up to 600°C. At higher temperatures, the PS-PVD coating had the highest reflectance. The importance of high reflectance differs between

engines. Depending on the amount of thermal radiation generated in the combustion chamber, either the columnar PS-PVD or nanostructured/conventional APS coatings have the best thermal insulation properties at temperatures above 650°C.

How is the heat flux from the combustion chamber influenced by TBCs with respect to their composition, microstructure, and sealed porosity?

In situ heat flux measurements indicated that plasma-sprayed YSZ coatings with the pores sealed with aluminium phosphate had higher heat fluxes than that of a steel reference, this being explained by the decreased reflectance caused by the sealer; all other studied TBCs had heat fluxes that were 0.2–4.7% lower. $Gd_2Zr_2O_7$ was the coating material that provided the best thermal insulation, due to its low thermal conductivity combined with high reflectance, followed by segmented YSZ. $La_2Zr_2O_7$ and conventional YSZ coatings were less effective, reducing the heat flux by 0.6% and 0.9%, respectively. The YSZ microstructure with the highest heat flux reduction was the segmented microstructure, followed by the conventional microstructured and the nanostructured coatings. However, the influence of microstructure type was small.

Is there a running-in period, with respect to thermal insulation properties, for TBCs inside a combustion chamber?

There is a running-in period for plasma-sprayed YSZ and $Gd_2Zr_2O_7$ coatings. In situ heat flux measurements indicated that the heat flux through these two TBCs decreased by 3% and 5%, respectively, during 5-h engine tests when the engine ran continuously at about 50% load. It took about 2–3 h for the heat flux to stabilize for these two coatings. The decreased heat flux was due to the growth of microcracks in the YSZ coating and to the growth of a large crack in the $Gd_2Zr_2O_7$ coating. The $La_2Zr_2O_7$ coating displayed no running-in behaviour like that of the other two TBCs.

6.3 Future work

Further potential improvements in the probe used for in situ heat flux measurements in the combustion chamber have been identified. More accurately positioning the thermocouples closer to the outer diameter of the shaft would reduce the risk of measurement errors. Redesigning the retainer that holds the probe in place would enable faster assembly/disassembly and faster measurements. Better-controlled water cooling with a larger water reservoir would enable longer test runs with a high and constant temperature gradient over the probe.

The redesigned probe could be used in further in situ studies of the thermal insulation properties of various TBCs and surface modifications. By correlating the in situ heat flux measurements to the thermal conductivity and reflectance results from Paper B, the importance of thermal radiation for the total heat flux could be better understood.

The TBCs exposed to engine exhaust conditions in Paper A were applied to a flat circular surface. The positioning of these samples in specially made holes in the exhaust manifolds resulted in certain problems. A limited number of samples could be tested simultaneously and the conditions may have differed between the positions. Another test method that solves these problems should be used in the future testing of TBCs for exhaust components. Short pipes, internally coated with TBCs, could be connected after each other in a row to form a long pipe. Exhaust from an engine would then be directed through the connected pipe sections, and the performance of the TBCs evaluated.

Evaluating how different types of microstructures influenced the thermal cycling lifetime found that high strain tolerance resulting from segmentation cracks or gaps between columnar grains had a positive effect. One coating process not included in the tests is suspension plasma spraying (SPS), which can be used to manufacture columnar microstructured coatings with low thermal conductivity. This coating method will be included in future tests.

Bibliography

[1] K. Holmberg, P. Andersson, N.-O. Nylund, K. Mäkelä, and A. Erdemir, “Global energy consumption due to friction in trucks and buses,” *Tribology International,* vol. 78, pp. 94-114, 10// 2014.

[2] A. J. Modi, “Experimental study of energy balance in thermal barrier coated diesel engine,” SAE Technical Paper 2012-01-0389, 2012, doi:10.4271/2012-01-0389.

[3] R. Kamo, N. Mavinahally, L. Kamo, W. Bryzik, and E. Schwartz., “Injection characteristics that improve performance of ceramic coated diesel engines,” SAE Technical Paper 1999-01-0972, 1999, doi:10.4271/1999-01-0972.

[4] E. Schwarz, E. Danielson, W. Bryzik, T. Keelan, and N. Hakim, “NATO qualification test of Detroit Diesel 8V71-TA engine at 530 bhp with advanced ceramic components,” SAE Technical Paper 2000-01-0524, 2000, doi:10.4271/2000-01-0524.

[5] M. Vittal, J. A. Borek, D. A. Marks, A. L. Boehman, D. A. Okrent, and A. P. Bentz, “The effects of thermal barrier coatings on diesel engine emissions,” *Journal of Engineering for Gas Turbines and Power,* vol. 121, no. 2, pp. 218-225, 1999.

[6] S. Jaichandar and P. Tamilporai, “Low heat rejection engines – An overview,” SAE Technical Paper 2003-01-0405, 2003, doi:10.4271/2003-01-0405.

[7] D. Vargas, “Thermal barrier coatings for efficient combustion,” Master thesis, KTH, School of Industrial Engineering and Management (ITM), Materials Science and Engineering, KTH, DiVA, diva2:759397, 2014.

[8] M. Ekström, “Oxidation and corrosion fatigue aspects of cast exhaust manifolds,” Doctoral thesis, KTH, School of Industrial Engineering and Management (ITM), Materials Science and Engineering, Mechanical Metallurgy, KTH Royal Institute of Technology, Stockholm, 0000-0001-5212-2227, 2015.

[9] D. R. Clarke and C. G. Levi, “Materials design for the next generation thermal barrier coatings,” *Annual Review of Materials Research,* vol. 33, no. 1, pp. 383-417, 2003.

[10] B.-C. Wu, E. Chang, S.-F. Chang, and D. Tu, “Degradation mechanisms of ZrO2–8 wt% Y2O3/Ni-22Cr-10Al-1Y thermal barrier coatings,” *Journal of the American Ceramic Society,* vol. 72, no. 2, pp. 212-218, 1989.

[11] R. Sobhanverdi and A. Akbari, “Porosity and microstructural features of plasma sprayed yttria stabilized zirconia thermal barrier coatings,” *Ceramics International,* vol. 41, no. 10, Part B, pp. 14517-14528, 12// 2015.

[12] P. L. Fauchais, Heberlein, J. V. R. and Boulos, M., *Thermal spray fundamentals from powder to part* Boston: Springer US 2014.

[13] M. Karger, R. Vaßen, and D. Stöver, “Atmospheric plasma sprayed thermal barrier coatings with high segmentation crack densities: Spraying process, microstructure and thermal cycling behavior,” *Surface and Coatings Technology,* vol. 206, no. 1, pp. 16-23, 10/15/ 2011.

[14] G. Trapaga, E. F. Matthys, J. J. Valencia, and J. Szekely, “Fluid flow, heat transfer, and solidification of molten metal droplets impinging on substrates: Comparison of numerical and experimental results,” *Metallurgical Transactions B,* vol. 23, no. 6, pp. 701-718, 1992.

[15] J. R. Davis, *Handbook of Thermal Spray Technology*. Materials Park: Materials Park: A S M International, 2004.

[16] J. A. Gan and C. C. Berndt, “Quantification and taxonomy of pores in thermal spray coatings by image analysis and stereology approach,” *Metallurgical and Materials Transactions A,* journal article vol. 44, no. 10, pp. 4844-4858, 2013.

[17] S. Kuroda and T. W. Clyne, “The quenching stress in thermally sprayed coatings,” *Thin Solid Films,* vol. 200, no. 1, pp. 49-66, 1991/05/01 1991.

[18] R. S. Lima and B. R. Marple, “Thermal spray coatings engineered from nanostructured ceramic agglomerated powders for structural, thermal barrier and biomedical applications: A review,” *Journal of Thermal Spray Technology,* journal article vol. 16, no. 1, pp. 40-63, 2007.

[19] J. Wu, H.-b. Guo, L. Zhou, L. Wang, and S.-k. Gong, “Microstructure and thermal properties of plasma sprayed thermal barrier coatings from nanostructured YSZ,” *Journal of Thermal Spray Technology,* vol. 19, no. 6, pp. 1186-1194, 2010.

[20] C. Zhou, N. Wang, and H. Xu, “Comparison of thermal cycling behavior of plasma-sprayed nanostructured and traditional thermal barrier coatings,” *Materials Science and Engineering: A,* vol. 452–453, pp. 569-574, 4/15/ 2007.

[21] H. Jamali, R. Mozafarinia, R. Shoja Razavi, and R. Ahmadi-Pidani, “Comparison of thermal shock resistances of plasma-sprayed nanostructured and conventional yttria stabilized zirconia thermal barrier coatings,” *Ceramics International,* vol. 38, no. 8, pp. 6705-6712, 12// 2012.

[22] R. S. Lima and B. R. Marple, “Nanostructured YSZ thermal barrier coatings engineered to counteract sintering effects,” *Materials Science and Engineering: A,* vol. 485, no. 1–2, pp. 182-193, 6/25/ 2008.

[23] V. E. Oliker, T. Y. Gridasova, and A. A. Pritulyak, “Effect of the porous structure of thermal-barrier coatings on their heat conductivity,” *Powder Metallurgy and Metal Ceramics,* vol. 47, no. 11, pp. 717-722, 2008.

[24] S. Ghosh, D. Teweldebrhan, J. R. Morales, J. E. Garay, and A. A. Balandin, “Thermal properties of the optically transparent pore-free nanostructured yttria-stabilized zirconia,” *Journal of Applied Physics,* vol. 106, no. 11, p. 113507, 2009.

[25] A. M. Limarga and D. R. Clarke, “The grain size and temperature dependence of the thermal conductivity of polycrystalline, tetragonal yttria-stabilized zirconia,” *Applied Physics Letters,* vol. 98, no. 21, p. 211906, 2011.

[26] H. B. Guo, R. Vaßen, and D. Stöver, “Atmospheric plasma sprayed thick thermal barrier coatings with high segmentation crack density,” *Surface and Coatings Technology,* vol. 186, no. 3, pp. 353-363, 9/1/ 2004.

[27] Z. Lu *et al.*, “Microstructure evolution and interface stability of thermal barrier coatings with vertical type cracks in cyclic thermal exposure,” *Journal of Thermal Spray Technology,* vol. 22, no. 5, pp. 671-679, 2013.

[28] U. Schulz *et al.*, “Some recent trends in research and technology of advanced thermal barrier coatings,” *Aerospace Science and Technology,* vol. 7, no. 1, pp. 73-80, 1// 2003.

[29] D. D. Hass, P. A. Parrish, and H. N. G. Wadley, “Electron beam directed vapor deposition of thermal barrier coatings,” *Journal of Vacuum Science and Technology A: Vacuum, Surfaces and Films,* vol. 16, no. 6, pp. 3396-3401, 1998.
[30] S. Rezanka, G. Mauer, and R. Vaßen, “Improved thermal cycling durability of thermal barrier coatings manufactured by PS-PVD,” *Journal of Thermal Spray Technology,* vol. 23, no. 1, pp. 182-189, 2014.
[31] L. Gao, H. Guo, L. Wei, C. Li, and H. Xu, “Microstructure, thermal conductivity and thermal cycling behavior of thermal barrier coatings prepared by plasma spray physical vapor deposition,” *Surface and Coatings Technology,* vol. 276, pp. 424-430, 8/25/ 2015.
[32] K. von Niessen, M. Gindrat, and A. Refke, “Vapor phase deposition using plasma spray-PVD™,” *Journal of Thermal Spray Technology,* vol. 19, no. 1, pp. 502-509, 2010.
[33] A. Hospach, G. Mauer, R. Vaßen, and D. Stöver, “Columnar-structured thermal barrier coatings (TBCs) by thin film low-pressure plasma spraying (LPPS-TF),” *Journal of Thermal Spray Technology,* vol. 20, no. 1, pp. 116-120, 2011.
[34] P. Nguyen, S. Harding, and S.-Y. Ho, “Experimental studies on slurry based thermal barrier coatings,” in *Proceedings of the 5th Australasian Congress on Applied Mechanics*, 2007, p. 545: Engineers Australia.
[35] A. Kawasaki and R. Watanabe, “Thermal fracture behavior of metal/ceramic functionally graded materials,” *Engineering Fracture Mechanics,* vol. 69, no. 14–16, pp. 1713-1728, 9// 2002.
[36] C. J. Brinker, G. C. Frye, A. J. Hurd, and C. S. Ashley, “Fundamentals of sol-gel dip coating,” *Thin Solid Films,* vol. 201, no. 1, pp. 97-108, 1991/06/05 1991.
[37] M. F.Shabir, S. Authars, S. Ganesan, R. Karthik, and S. K. Madhan, “Low heat rejection engines – review,” SAE Technical Papers 2010-01-1510, 2010,doi.org/10.4271/2010-01-1510.
[38] S. Mahade, N. Curry, S. Björklund, N. Markocsan, P. Nylén, and R. Vaßen, “Functional performance of Gd2Zr2O7/YSZ multi-layered thermal barrier coatings deposited by suspension plasma spray,” *Surface and Coatings Technology*.
[39] S. Bose, “Chapter 7 – Thermal barrier coatings (TBCs),” in *High Temperature Coatings* Burlington: Butterworth-Heinemann, 2007, pp. 155-232.
[40] R. Vassen, X. Cao, F. Tietz, D. Basu, and D. Stöver, “Zirconates as New Materials for Thermal Barrier Coatings,” *Journal of the American Ceramic Society,* vol. 83, no. 8, pp. 2023-2028, 2000.
[41] H. G. Scott, “Phase relationships in the zirconia-yttria system,” *Journal of Materials Science,* vol. 10, no. 9, pp. 1527-1535, 1975.
[42] S. Mahade, “Functional performance of gadolinium zirconate/yttria stabilized zirconia multi-layered thermal barrier coatings,” Licentiate dissertation, University West, Department of Engineering Science, Division of Subtractive and Additive Manufacturing, University West, 2016.
[43] R. Vaßen, M. O. Jarligo, T. Steinke, D. E. Mack, and D. Stöver, “Overview on advanced thermal barrier coatings,” *Surface and Coatings Technology,* vol. 205, no. 4, pp. 938-942, 11/15/ 2010.
[44] G. Moskal *et al.*, “Characterization of microstructure and thermal properties of Gd2Zr2O7-type thermal barrier coating,” *Journal of the European Ceramic Society,* vol. 32, no. 9, pp. 2025-2034, 7// 2012.
[45] R. M. Leckie, S. Krämer, M. Rühle, and C. G. Levi, “Thermochemical compatibility between alumina and ZrO2–GdO3/2 thermal barrier coatings,” *Acta Materialia,* vol. 53, no. 11, pp. 3281-3292, 6// 2005.
[46] X. Q. Cao, R. Vassen, W. Jungen, S. Schwartz, F. Tietz, and D. Stöver, “Thermal stability of lanthanum zirconate plasma-sprayed coating,” *Journal of the American Ceramic Society,* vol. 84, no. 9, pp. 2086-2090, 2001.
[47] K. N. Lee, R. A. Miller, and N. S. Jacobson, “New generation of plasma-sprayed mullite coatings on silicon carbide,” *Journal of the American Ceramic Society,* vol. 78, no. 3, pp. 705-710, 1995.
[48] H. Salimijazi *et al.*, “Plasma sprayed coating using mullite and mixed alumina/silica powders,” *Journal of Thermal Spray Technology,* vol. 21, no. 5, pp. 825-830, 2012.
[49] H. Schneider, J. Schreuer, and B. Hildmann, “Structure and properties of mullite—A review,” *Journal of the European Ceramic Society,* vol. 28, no. 2, pp. 329-344, // 2008.
[50] R. Soltani, H. Samadi, E. Garcia, and T. W. Coyle, “Development of alternative thermal barrier coatings for diesel engines,” SAE Technical Papers 2005-01-0650, 2005, doi:10.4271/2005-01-0650.
[51] H. Samadi and E. García, “Thermal conductivity of plasma sprayed forsterite/mullite coatings,” *Ceramics International,* vol. 40, no. 9, Part A, pp. 13995-13999, 11// 2014.
[52] D. R. Tree, D. C. Oren, T. M. Yonushonis, and P. D. Wiczynski, “Experimental measurements on the effect of insulated pistons on engine performance and heat transfer,” SAE Technical Papers 960317, 1996, doi:10.4271/960317.
[53] A. J. Scharman and T. M. Yonushonis, “Ceramic thermal barrier coating for rapid thermal cycling applications,” ed: Google Patents, 1994.
[54] P. M. Pierz, “Thermal barrier coating development for diesel engine aluminum pistons,” *Surface and Coatings Technology,* vol. 61, no. 1, pp. 60-66, 1993/12/03 1993.
[55] K. Kokini, Y. R. Takeuchi, and B. D. Choules, “Surface thermal cracking of thermal barrier coatings owing to stress relaxation: zirconia vs. mullite,” *Surface and Coatings Technology,* vol. 82, no. 1, pp. 77-82, 1996/07/01 1996.
[56] H. Wang and H. Herman, “Thermomechanical properties of plasma-sprayed oxides in the MgO-Al2O3-SiO2 system,” *Surface and Coatings Technology,* vol. 42, no. 3, pp. 203-216, 1990/12/15 1990.
[57] M. Gupta, *Design of thermal barrier coatings A modelling approach* Springer International Publishing: Imprint: Springer, 2015.
[58] G. Qian, T. Nakamura, and C. C. Berndt, “Effects of thermal gradient and residual stresses on thermal barrier coating fracture,” *Mechanics of Materials,* vol. 27, no. 2, pp. 91-110, 2// 1998.
[59] M. Ekström, A. Thibblin, A. Tjernberg, C. Blomqvist, and S. Jonsson, “Evaluation of internal thermal barrier coatings for exhaust manifolds,” *Surface and Coatings Technology,* vol. 272, no. 0, pp. 198-212, 6/25/ 2015.
[60] D. M. Zhu, R. Miller, “Evaluation of oxidation damage in thermal barrier coating systems,” Technical memo 1996. National aeronautics and space administration Cleveland OH Lewis Research Center.
[61] D. R. Clarke and S. R. Phillpot, “Thermal barrier coating materials,” *Materials Today,* vol. 8, no. 6, pp. 22-29, 6// 2005.

[62] C. G. Levi, “Emerging materials and processes for thermal barrier systems,” *Current Opinion in Solid State and Materials Science,* vol. 8, no. 1, pp. 77-91, 1// 2004.
[63] D. D. Hass, A. J. Slifka, and H. N. G. Wadley, “Low thermal conductivity vapor deposited zirconia microstructures,” *Acta Materialia,* vol. 49, no. 6, pp. 973-983, 4/2/ 2001.
[64] T. E. Strangman and D. Raybould, “Lower conductivity barrier coating,” ed: Google Patents, 2002.
[65] W. G. Mao, Y. C. Zhou, L. Yang, and X. H. Yu, “Modeling of residual stresses variation with thermal cycling in thermal barrier coatings,” *Mechanics of Materials,* vol. 38, no. 12, pp. 1118-1127, 12// 2006.
[66] M. B. Beardsley, P. G. Happoldt, K. C. Kelley, E. F. Rejda, and D. F. Socie, “Thermal barrier coatings for low emission, high efficiency diesel engine applications,” SAE Technical Papers 1999-01-2255, 1999, doi:10.4271/1999-01-2255.
[67] R. Dutton, R. Wheeler, K. S. Ravichandran, and K. An, “Effect of heat treatment on the thermal conductivity of plasma-sprayed thermal barrier coatings,” *Journal of Thermal Spray Technology,* journal article vol. 9, no. 2, pp. 204-209, 2000.
[68] S. Paul, A. Cipitria, S. A. Tsipas, and T. W. Clyne, “Sintering characteristics of plasma sprayed zirconia coatings containing different stabilisers,” *Surface and Coatings Technology,* vol. 203, no. 8, pp. 1069-1074, 1/15/ 2009.
[69] H. E. Evans, “Oxidation failure of TBC systems: An assessment of mechanisms,” *Surface and Coatings Technology,* vol. 206, no. 7, pp. 1512-1521, 12/25/ 2011.
[70] J. I. Eldridge, C. M. Spuckler, K. W. Street, and J. R. Markham, “Infrared radiative properties of yttria–stabilized zirconia thermal barrier coatings,” in *26th Annual Conference on Composites, Advanced Ceramics, Materials, and Structures: B: Ceramic Engineering and Science Proceedings*: John Wiley & Sons, Inc., 2008, pp. 417-430.
[71] R. Siegel and C. M. Spuckler, “Analysis of thermal radiation effects on temperatures in turbine engine thermal barrier coatings,” *Materials Science and Engineering: A,* vol. 245, no. 2, pp. 150-159, 5/1/ 1998.
[72] J. Manara, M. Arduini-Schuster, H. J. Rätzer-Scheibe, and U. Schulz, “Infrared-optical properties and heat transfer coefficients of semitransparent thermal barrier coatings,” *Surface and Coatings Technology,* vol. 203, no. 8, pp. 1059-1068, 1/15/ 2009.
[73] K. Mendera, “Effectiveness of plasma sprayed coatings for engine combustion chamber,” SAE Technical Papers 2000-01-2982, 2000 doi:10.4271/2000-01-2982.
[74] D. Wang, X. Huang, and P. Patnaik, “Design and modeling of multiple layered TBC system with high reflectance,” *Journal of Materials Science,* vol. 41, no. 19, pp. 6245-6255, 2006.
[75] M. J. Kelly, D. E. Wolfe, J. Singh, J. Eldridge, D.-M. Zhu, and R. Miller, “Thermal barrier coatings design with increased reflectivity and lower thermal conductivity for high-temperature turbine applications,” *International Journal of Applied Ceramic Technology,* vol. 3, no. 2, pp. 81-93, 2006.
[76] S. Gu, T. J. Lu, D. D. Hass, and H. N. G. Wadley, “Thermal conductivity of zirconia coatings with zig-zag pore microstructures,” *Acta Materialia,* vol. 49, no. 13, pp. 2539-2547, 8/1/ 2001.
[77] L. Wang, J. I. Eldridge, and S. M. Guo, “Thermal radiation properties of plasma-sprayed Gd2Zr2O7 thermal barrier coatings,” *Scripta Materialia,* vol. 69, no. 9, pp. 674-677, 11// 2013.
[78] V. Merzlikin, V. Timonin, M. Ojeda, and O. Sidorov, “New selectively absorbing and scattering heat-insulating coatings of the combustion chamber for low-heat-rejection diesel,” SAE Technical Papers 2007-01-1755, 2007, doi:10.4271/2007-01-1755.
[79] D. W. Dickey, “The effect of insulated combustion chamber surfaces on direct-injected diesel engine performance, emissions and combustion,” SAE Technical Papers 890292, 1989, doi:10.4271/890292.
[80] C. G. S. P. Ramu, “Effect of ZrO2-Al2O3 and SiC coating on diesel engine to study the combustion and emission characteristics,” SAE Technical Papers 2009-01-1435, 2009, doi:10.4271/2009-01-1435.
[81] S. Kobori, T. Kamimoto, and M. T. Luta, “Combustion in low-heat-rejection diesel engines,” *JSME international journal. Ser. 2, Fluids engineering, heat transfer, power, combustion, thermophysical properties,* vol. 35, no. 1, pp. 1-9, 1992.
[82] R. B. GmbH, *Automotive Handbook*. Wiley, 2011.
[83] G. Woschni, W. Spindler, and K. Kolesa, “Heat insulation of combustion chamber walls — A measure to decrease the fuel consumption of I.C. engines?,” SAE Technical Papers 870339, 1987, doi:10.4271/870339.
[84] Y. Tsutsumi, K. Nomura, and N. Nakamura, “Effect of Mirror-Finished Combustion Chamber on Heat Loss,” SAE Technical Papers 902141, 1990, doi:10.4271/902141.
[85] R. S. Bunker, “The Effect of Thermal Barrier Coating Roughness Magnitude on Heat Transfer With and Without Flowpath Surface Steps,” no. 37181b, pp. 1-10, 2003.
[86] M. Marr, J. S. Wallace, S. Memme, S. Chandra, L. Pershin, and J. Mostaghimi, “An Investigation of Metal and Ceramic Thermal Barrier Coatings in a Spark-Ignition Engine,” *SAE Int. J. Engines,* vol. 3, no. 2, pp. 115-125, 2010.
[87] M. A. Marr, J. S. Wallace, L. Pershin, S. Chandra, and J. Mostaghimi, “Preliminary testing of metal-based thermal barrier coating in a spark-ignition engine,” *Journal of Engineering for Gas Turbines and Power,* vol. 132, no. 7, pp. 072806-072806-7, 2010.
[88] S. Memme and J. S. Wallace, “The influence of thermal barrier coating surface roughness on spark-ignition engine performance and emissions,” no. 55096, pp. 893-905, 2012.
[89] S. Memme, “The influence of thermal barrier coating surface roughness on spark ignition engine performance and emissions,” Master Thesis, Mechanical and Industrial Engineering, University of Toronto, 2012.
[90] R. E. Taylor, “Thermal conductivity determinations of thermal barrier coatings,” *Materials Science and Engineering: A,* vol. 245, no. 2, pp. 160-167, 5/1/ 1998.
[91] S. Pisasale, “Heat flux measurement device: Designing an experimental system for determining the effectiveness of thermal barrier coating inside a combustion chamber,” Master Thesis, KTH Royal Institute of Technology, 2015.
[92] S. Kianzad, “Measurement of thermal insulation properties of TBC inside the combustion chamber,” Master Thesis, Department of Engineering Sciences and Mathematics, Luleå University of Technology, urn:nbn:se:ltu:diva-61917, 2017.
[93] M. Gupta, N. Curry, P. Nylén, N. Markocsan, and R. Vaßen, “Design of next generation thermal barrier coatings — Experiments and modelling,” *Surface and Coatings Technology,* vol. 220, no. 0, pp. 20-26, 4/15/ 2013.

[94] D. Zhu, J. A. Nesbitt, C. A. Barrett, T. R. McCue, and R. A. Miller, “Furnace cyclic behavior of plasma-sprayed zirconia-yttria and multi-component rare earth oxide doped thermal barrier coatings – NASA/TM-2002-211690,” NASA Glenn Research Center, 2002.
[95] N. Curry, K. VanEvery, T. Snyder, and N. Markocsan, “Thermal conductivity analysis and lifetime testing of suspension plasma-sprayed thermal barrier coatings,” *Coatings,* vol. 4, no. 3, p. 630, 2014.
[96] R. Eriksson, H. Brodin, S. Johansson, L. Östergren, and X.-H. Li, “Influence of isothermal and cyclic heat treatments on the adhesion of plasma sprayed thermal barrier coatings,” *Surface and Coatings Technology,* vol. 205, no. 23–24, pp. 5422-5429, 9/25/ 2011.
[97] R. Eriksson, “Thermal barrier coatings: Durability assessment and life prediction,” Doctoral Thesis 1527, Linköping University Electronic Press, Linköping, 2013.
[98] M. Ekström and S. Jonsson, “High-temperature mechanical- and fatigue properties of cast alloys intended for use in exhaust manifolds,” *Materials Science and Engineering: A,* vol. 616, pp. 78-87, 10/20/ 2014.
[99] M. Ekström, P. Szakalos, and S. Jonsson, “Influence of Cr and Ni on high-temperature corrosion behavior of ferritic ductile cast iron in air and exhaust gases,” *Oxidation of Metals,* vol. 80, no. 5, pp. 455-466, 2013.
[100] W. Ma and H. Dong, “2 – Ceramic thermal barrier coating materials,” in *Thermal Barrier Coatings*: Woodhead Publishing, 2011, pp. 25-52.
[101] H. Chen, X. Zhou, and C. Ding, “Investigation of the thermomechanical properties of a plasma-sprayed nanostructured zirconia coating,” *Journal of the European Ceramic Society,* vol. 23, no. 9, pp. 1449-1455, 8// 2003.
[102] J. F. Shackelford and W. Alexander, “CRC Materials science and engineering handbook (3rd Edition),” ed: Taylor & Francis, pp. 50-52.
[103] (2015, Jan 22). *The mineral website*. Available: http://webmineral.com/data/Forsterite.shtml#.VMDxWMaSX4g.
[104] (2015, Jan 22). *Inframat Advanced Materials*. Available: http://www.advancedmaterials.us/4039OR-8601.htm.
[105] L. Kong, I. Karatchevtseva, D. J. Gregg, M. G. Blackford, R. Holmes, and G. Triani, “A novel chemical route to prepare La2Zr2O7 pyrochlore,” *Journal of the American Ceramic Society,* vol. 96, no. 3, pp. 935-941, 2013.
[106] D. Zhu, R. A. Miller, , “Influence of high cycle thermal loads on thermal fatigue behavior of thick thermal barrier coatings – NASA-TP-3676 “ Army Research Lab. NASA Lewis Research Center 97N20182; 19970018102; 1997.
[107] A. Stuke *et al.*, “Optimizing of the reflectivity of air plasma sprayed ceramic thermal barrier coatings,” in *Advanced Ceramic Coatings and Interfaces II: Ceramic and Engineering Science Proceedings, Volume 28, Issue 3*: John Wiley & Sons, Inc., 2009, pp. 99-113.
[108] B. J. Zhang, B. X. Wang, and C. Y. Zhao, “Microstructural effect on the radiative properties of YSZ thermal barrier coatings (TBCs),” *International Journal of Heat and Mass Transfer,* vol. 73, pp. 59-66, 6// 2014.
[109] L. Li and D. R. Clarke, “Effect of CMAS infiltration on radiative transport through an EB-PVD thermal barrier coating,” *International Journal of Applied Ceramic Technology,* vol. 5, no. 3, pp. 278-288, 2008.
[110] A. M. Limarga and D. R. Clarke, “Characterization of electron beam physical vapor-deposited thermal barrier coatings using diffuse optical reflectance,” *International Journal of Applied Ceramic Technology,* vol. 6, no. 3, pp. 400-409, 2009.
[111] D. M. Dryden, G. L. Tan, and R. H. French, “Optical properties and van der Waals–London dispersion interactions in Berlinite aluminum phosphate from vacuum ultraviolet spectroscopy,” *Journal of the American Ceramic Society,* vol. 97, no. 4, pp. 1143-1150, 2014.